TÉCNICO LISBOA

Influence of wind on the electrical energy production of solar plants

Carlos Bernardo Capritos Lopes

Thesis to obtain the Master of Science Degree in

Electrical and Computer Engineering

Supervisors: Prof. João Paulo Neto Torres
Prof. Carlos Alberto Ferreira Fernandes

Examination Committee

Chairperson: Prof. Francisco André Corrêa Alegria
Supervisor: Prof. João Paulo Neto Torres
Member of the Committee: Prof. António Carlos De Campos Simões Baptista

September 2021

I declare that this document is an original work of my own authorship and that it fulfills all the requirements of the Code of Conduct and Good Practices of the Universidade de Lisboa.

Acknowledgments

First of all, I would like to thank my sister, Bárbara, for all her guidance before and throughout this academic journey. Without her advises and help, the stumbling blocks that crossed this path would have been much harder to face.

Then, an outstanding thank you to my parents, Carlos and Regina, for always encouraging me and for the education they provided me. Without them, I would not have had the pleasure of being part of this incredible institution that is Instituto Superior Técnico.

A special thank you to Professor João Paulo Neto Torres, for receiving me under his supervision and for his support in the most essential aspects regarding the making of this dissertation.

Last but not least, I would like to thank my friends António, Diogo, Gonçalo and Guilherme for always being by my side, for all the laughs and uncountable hours of study and joy we have shared in the last years. Without them, this adventure would have lost all its glow.

Abstract

In the pursuit of better understanding the various worlds behind solar photovoltaic methods and technologies, researchers rely on incessant investigations with the aim of guaranteeing an effective energy demand response to an ever-growing world population that fights climate change. Solar energy, as a clean source of energy, plays a relevant role in this much desired (r)evolution.

When talking about photovoltaics, despite the multiple studies on parameters that affect the operation of solar panels, concrete knowledge on this matter is still in an incipient stage and precise data remains dispersed, given the mutability of outer factors beyond technology-related properties, hence the difficulties associated with their exploration. Wind is one of them. Wind loads can affect the temperature of photovoltaic modules, whose efficiency is reduced when higher temperatures are reached. With this in mind, the viability of wind as a natural cooling mechanism for solar plants and its influence on their electrical energy production is studied in this thesis.

Some appropriate results were achieved: depending on the module temperature prediction model used and on the photovoltaic technology in question, solar panels are foreseen to be up to approximately 3% more productive for average wind speeds and up to almost 7% more productive for higher wind speeds. Taking into consideration that wind speed values were collected in the close vicinity of the modules, these results can be proven to be even higher.

That being said, this dissertation intends to contribute with accurate insights about wind influence on electrical energy production of solar plants.

Keywords

Wind Flow; Temperature Prediction; Photovoltaic Panel; Output Power; Computational Fluid Dynamics; CAD Models.

Resumo

O incessante aumento populacional verificado nas últimas decadas e as consequências que dele advêm têm levado a uma crescente necessidade energética. Como tal, têm sido desenvolvidos diversos estudos no sentido de aproveitar as fontes de energia existentes e tornar as tecnologias mais eficientes. A energia solar, como energia limpa, desempenha um papel fundamental nesta tão necessária e desejada (r)evolução.

No que toca à energia solar fotovoltaica, apesar dos variados ensaios sobre os fatores que influenciam a operação dos painéis fotovoltaicos, os seus contornos encontram-se ainda relativamente pouco definidos, dada a elevada mutabilidade dos parâmetros além-tecnologia. Um deles é o vento, que pode variar a temperatura dos painéis, cuja eficiência é reduzida com o seu aumento. Por conseguinte, nesta tese, estuda-se a viabilidade do vento como mecanismo natural de arrefecimento de painéis solares e o seu efeito na produção de energia elétrica das centrais solares.

Foram obtidos resultados relevantes: dependendo do modelo de previsão de temperatura e da tecnologia em questão, a potência de saída pode revelar-se superior em até aproximadamente 3% para velocidades médias do vento e chegar até quase aos 7% para velocidades do vento elevadas. Uma vez que os valores da velocidade do vento foram registados para uma vizinhança imediata dos módulos solares, os resultados finais podem mostrar-se ainda mais elevados.

Assim sendo, esta dissertação pretende fornecer um contributo significativo no que concerne ao estudo da influência do vento na produção de energia elétrica das centrais solares.

Palavras Chave

Fluxo de Vento; Temperatura Prevista; Painel Fotovoltaico; Potência de Saída; Dinâmica de Fluidos Computacional; Modelos CAD.

Contents

List of Figures

List of Tables

Acronyms

CAD	Computer-Aided Design
CFD	Computational Fluid Dynamics
DSSC	Dye-Sensitized Solar Cells
ECMWF	European Centre for Medium range Weather Forecast
FF	Fill Factor
IPMA	Instituto Português do Mar e da Atmosfera
MJSC	Multi-Junction Solar Cells
MPP	Maximum Power Point
NOCT	Nominal Operating Cell Temperature
PV	Photovoltaic
QDSC	Quantum Dots Solar Cells
RANS	Reynolds-Average Navier Stokes
RMSE	Root Minimum Squared Error
SA	Standard Approach
STC	Standard Test Conditions

Nomenclature

A_{cell}	Solar Cell Area
Al	Aluminium
AM	Air Mass
As	Arsenide
a-Si	Amorphous Silicon
B	Boron
CdTe	Cadmium Telluride
CIGS	Copper Indium Gallium Selenide
CIS	Copper Indium Selenide
C_0	Constant Dependent on T_C
C_1	Coefficient of Temperature of I_{PV}
D	Pipe Diameter
d	Inter Row Spacing
E_c	Conduction Band Energy
E_g	Bandgap Energy
E_F	Fermi Level Energy
E_{ph}	Photon Energy
E_v	Valence Band Energy
FF	Fill Factor

G	Irradiance
Ga	Gallium
GaAs	Gallium Arsenide
Ge	Germanium
G_m	Module Plane Irradiance
G_{ref}	Reference Irradiance
G_{NOCT}	Irradiance at NOCT Conditions
h	Model Height
h_w	Wind Convection Coefficient
$h_{\text{w,NOCT}}$	Wind Convection Coefficient at NOCT Conditions
I	Current
I	Turbulence Intensity
I_{cell}	Solar Cell Current
I_D	Diode Current
I_{mpp}	Maximum Power Point Current
In	Indium
I_{PV}	Current Generated by Light
I_S	Diode Reverse Saturation Current
I_{SC}	Short-circuit Current
$I_{\text{SC}_{ref}}$	Reference Short-circuit Current
k	Boltzmann Constant
k	Ross Coefficient
k	Turbulent Kinetic Energy
L	Module Length
l	Model Length

l	Turbulent Length Scale
M	Number of Cells
m_d	Module Deflection
n	Number of Free Electrons
n	Diode Ideality Factor
N_A	Density of Negatively Charged Acceptor Ions
N_c	Conduction Band Density of States
N_D	Density of Positively Charged Donor Ions
n_i	Intrinsic Concentration
N_v	Valence Band Density of States
P	Phosphorus
P	Pressure
p	Number of Free Holes
P_{max}	Maximum Power Point Power
P_{mpp}	Nominal Power
p-Si	Polycristalline (Silicon Based)
q	Electronic Charge
R	Resistance
R	Correlation Coefficient
Re	Reynolds Number
R_P	Parallel Resistance
R_S	Series Resistance
Sb	Antimony
Si	Silicon
T	Temperature

T_a Ambient Temperature

$T_{\text{a,NOCT}}$ Ambient Temperature at NOCT Conditions

T_c Cell Temperature

T_m Module Temperature

T_{NOCT} Temperature at NOCT Conditions

T_{STC} Temperature at STC

U Voltage

U_D Diode Voltage

U_{PV} Heat Exchange Coefficient for Module Surface

U_T Thermal Voltage

U_0 Coefficient of Koehl Model

U_1 Coefficient of Koehl Model

V Fluid Velocity

V_b Electrostatic Potential Difference

V_C Reverse Breakdown Voltage

V_{cell} Cell Voltage

V_F Forward Diode Bias Voltage

V_{mpp} Maximum Power Point Voltage

V_{OC} Open-circuit Current

V_w Wind Speed at 10m

v_t Turbulent Viscosity

v' Root Mean Square of Turbulent Velocity Fluctuations

w Module Width

W_{avg} Average Average Wind Speed

W_{avg_1} Average Wind Speed – Meteored

W_{max} Average Maximum Wind Speed

W_{max} Average Average Wind Speed

W_{max_1} Maximum Wind Speed – Meteored

W_{max_2} Maximum Wind Speed – IPMA

W_{speed} Wind Speed

$W_{\text{speed}_{ref}}$ Wind Speed at z_{ref}

z Height

z_{ref} Reference Height

α Absorptance

β_{STC} Temperature coefficient of maximum power

ΔT Difference between T_C and T_a

ϵ Turbulent Dissipation Rate

η Efficiency

η Fluid Dynamic Viscosity

η_{STC} Efficiency at STC Conditions

λ Wavelength

ω Solar Radiation Angle

ρ Fluid Density

τ Transmittance

θ Module Inclination

1

Introduction

Contents

1.1 Motivation

Throughout the last years, the urge to reduce the usage of fossil fuels has been arising substantially, putting the conventional energy sources under a lot of pressure. Herewith, the demand for renewable energies is constantly increasing as a consequence of their significance as an alternative to the aforementioned sources. The five major renewable energy resources are wind, hydro, geothermal, biomass and solar. With their never-ending stamp at human scale, they play an imperative role in the ecological footprint, continually giving rise to new projects, new initiatives and also political decisions all over the world, seeking a solid environmental sustainability for the years yet to come [1].

That being said, a much more fruitful use of the renewable resources is crucial for answering the needs of populations and modern societies. In such a way, an ever-developing work has to be carried out by the many renewable related industries in order to improve effectiveness and efficiency.

Amongst all the renewables, the usage of solar energy, although its recognized potential, still represents a small portion of the circle graph [2] – a situation expected to change in the upcoming years [3]. With emerging solar Photovoltaic (PV) technologies that show higher efficiencies and less costs, the referred fact is promised to change. With this in mind, as it can be considered that photovoltaics are still in an incipient phase due to their limitations in what concerns efficiency, several researches are on course in order to improve the operation of solar cells, either by, e.g., changing the designs, the structures or the materials, hence amplifying the reliability, spread and range of PV systems.

With this in mind, this dissertation is suggested with the aim of contributing to the growth of solar photovoltaic technology in the sense that a wider knowledge of how external factors affect efficiency and maintenance of solar plants empowers a general perspective of project sizing and forthcoming topics of interest.

1.2 Objectives

As above-mentioned, this work comes up as an attempt of studying the influence of external factors on the performance of PV modules on solar plants, namely, **wind**.

Facing many issues to what efficiency is concerned, PV panels are known to have their operation affected by temperature – ambient temperature and module temperature. Accordingly, higher temperatures are known to reduce the power output of PV modules, as it will be further explained in the next chapter. High temperatures also represent a problem regarding panels lifetime, since that overheating can lead to destructive effects, such as cell or glass cracking, melting of solder or degradation of the solar cells. This being the case, several cooling systems have been studied over the years, in order to avoid the issues aforesaid, being that some of them actually achieved relevant results. A consequent factor of these systems is an increase of investment and maintenance costs – a question to get around.

Therefore, wind, being a natural and free-of-cost resource, emerges as a possible alternative to them. Nowadays, wind is still neglected when predicting modules temperatures, which can be known because the Standard Approach (SA) does not take wind variables into consideration. This has been proven to be far-fetched and some efforts have been made to change this procedure. With the purpose of improving guidelines for solar photovoltaic practices, distinct researchers have been trying to elaborate panel temperature prediction models that take wind data into account, as it will be shown in chapter 2.

Considering what was previously stated, the work performed and exploited in this thesis aims to:

- Identify the variation of modules temperature according to each panel temperature prediction model;
- Study of this variation regarding various PV technologies;
- Verify the impact of different wind speeds in the variation of modules temperature;
- Examine how variations of panels temperature influence the output power of each module;
- Investigate the viability of wind as a natural cooling mechanism for solar plants.

1.3 Outline

After a brief introduction on the present dissertation, an overview on the organization of the following chapters is given.

This document is organized into six chapters. This first one, Introduction, introduces the thematic and the work that is going to be developed. In the second chapter, State of the Art, solar cells history, operation and characteristics are detailed; studies performed by other researchers that were considered relevant to this thesis are also showcased. The next chapter, Methodologies, contains information on the methods that were chosen with the aim of accomplishing the tasks proposed above. The fourth chapter, Computational Fluid Dynamics, has all the data related to the steps that precede computational simulations. Chapter five, Experimental Results, deals with all the simulations results and calculations that come up from them. Finally, the last chapter, Conclusions, highlights the conclusions and some future work.

The second chapter is divided into four main topics. Firstly, an initial contextualization of solar photovoltaic technology is made; then the photovoltaic effect is explained; right after, the operation of solar cells is detailed, being this the more extensive section of chapter; to finish it, the related studies are elaborated and significant points that will be fundamental to this research are mentioned. The third chapter is also divided into four matters. The first one indicates the theoretical foundations used; the second one the cell temperature prediction models employed to know the panels temperatures variations; the third

exposes the softwares adopted and the last one the reference data taken into consideration, such as meteorological conditions and solar cells parameters. Coincidentally, the fourth chapter is also divided into four contents. It begins with aspects related to the creation of photovoltaic arrays via a software; then it is given some information on wind tunnels and their functionalities; the following section is about meshing of the geometries and the last one includes the solver setup to solve simulations. The fifth chapter is split into three phases. The first is the analysis of computational simulations and data collected; it is followed by the calculations of temperature for the solar panels according to the different prediction models; to close the fifth chapter, the output power variation calculations produced by temperatures variation are displayed. The last chapter has two sections. In the first one, some conclusions are drawn regarding the work developed throughout this dissertation; in the final one, suggestions concerning the future work that can be performed are proposed.

2

State of the Art

Contents

In this chapter, it is given a relatively brief insight on the history and operation of solar photovoltaic technology, intending to allow a better understanding of the work presented in this document. Technical issues directly related to the influence of wind and other meteorological parameters beyond solar radiation are delved into further up in this chapter, starting in section Related Studies.

2.1 First Steps of Solar Photovoltaic Technology

It can be said that human beings have been using solar energy since the 7th century B.C., when it was used to light fires with magnifying glass materials, but it was only by the end of the Industrial Revolution, in 1839, that the French Edmond Becquerel performed several experiments that led him to the discovery and first demonstration of the photovoltaic effect, which will be explained right after, in section 2.2. By the decade of 1860, the French Mathematician August Mouchet presented his first solar steam engine, which he considered as not viable from the economic point of view due to the very low coal prices by that time. He was the first to publish a book on solar energy, *La chaleur solaire et ses applications industrielles*, in 1878 [4].

By the time of 1873, Willoughby Smith discovered the photoconductivity of selenium and, in 1883, the American Charles Fritts created the first solar cell from selenium wafers. In 1954, at Bell Labs, Daryl Chapin, Calvin Fuller and Gerald Pearson developed the first silicon (Si) photovoltaic cell with the capability of converting enough sun's energy into power to run everyday electrical equipment, giving birth to Photovoltaic Technology [5]. At first, they achieved an efficiency of 4% and were able to reach the significant value of 11% later.

From then to today's scenario, solar cells and PV technology have undergone enormous progress in therms of efficiency, reliability, operation, fabrication techniques and materials used, changing the way we live and the way we approach solar energy. It is now a commonly used technology with an unthinkable likelihood of growth through the upcoming years [1].

2.2 Photovoltaic Effect

Photovoltaic effect is the process that describes the conversion of light energy into electricity. It can be defined as the generation of a voltage and current when radiation ionizes the region between two layers of a semiconductor. It is characterized by a self-generated electromotive force and current that can deliver power to a load [6]. Photovoltaic effect is analogous to photoelectric effect; the biggest difference between them is that, in the phenomenon first-mentioned, the excited charge carrier remains within the material and, in the second one, the excitation of an electron causes its ejection out of the material.

In order to better understand the photovoltaic effect, it is convenient to know that solar cells absorb

light beams of electromagnetic radiation – photons – that derive from the sunlight. Photon's energy (E_{ph}) is inversely proportional to its wavelength (λ), hence, for the photovoltaic effect to happen, the energy of the incident photon needs to be equal or higher than the semiconductor's bandgap energy (E_g). If so, the photon will be absorbed by the semiconductor, resulting in the transfer of electrons from the valence band to the conduction band – a hole is created in the valence band and an electron-hole pair is established. This behavior will be further analyzed in section 2.3. In the case of the photon's energy being higher than the demanded energy to excite the electrons, the excess energy available causes the kinetic energy of the generated carrier to increase, since the charge carrier dissipates its excess energy by collisions with the medium [7], thus warming up the solar cells, lowering their efficiency.

2.3 Solar Cells, Semiconductors and P-N Junctions

A solar or a photovoltaic cell is a device that converts photon energy from the sun into electrical energy, flowing in an external circuit. Having this purpose, it needs to fulfill two functions: photo-generation of charge carriers (electrons and holes) in a light-absorbing material, and separation of the charge carriers to a conductive contact that will transmit the electricity – the so-called photoelectric effect [8].

Likewise light absorption, energy migration and carrier production make up one aspect of photovoltaic behavior, it is equally necessary for the production of a useful photovoltaic device the presence of a semiconductor junction. Semiconductors are the core of a solar cell. They are crystalline solids and they are categorized by their electrical conductivity, having an order of magnitude between conductors (10^5 to 10^8 S/m) and nonconductors or insulators (10^{-16} to 10^{-7} S/m). Despite the comparison, semiconductors have a central characteristic: the semiconductor's resistance varies with an inverse dependence on the temperature, which means that if the temperature rises, the semiconductor's resistance decreases and vice-versa.

Semiconductors are split in two categories: intrinsic and extrinsic. The first ones are considered to be semiconductors in their pure natural form, not having any impurity – the process of adding impurities to a semiconductor is called doping. Between these, silicon (Si) and germanium (Ge) are the most common, which are most frequently used in the manufacturing of transistors, diodes and other electronic components. In what concerns the second type, the opposite happens – impurities are added. This phenomenon entails a great increase of conductivity due to an increased number of electrons or holes, corresponding to two types of extrinsic semiconductors: N-type and P-type, respectively. Regarding the first one, the doping of an intrinsic semiconductor with pentavalent elements – they have 5 electrons in their valence shell – contributes with free electrons to the semiconductor (donor case). Some examples of pentavalent impurities are Phosphorus (P), Arsenic (As), Antimony (Sb). Respecting the second one, the addition of trivalent impurities – 3 electrons in their valence shell – results in a lack of valence

electrons because the doping atom establishes covalent bonds with only three neighboring atoms, generating a hole in the bond with the fourth atom (acceptor case). Aluminium (Al), Boron (B), Indium (In) and Gallium (Ga) are examples of trivalent elements.

As shown in equation (2.1), the number of free electrons, n, in the conduction band of a semiconductor is given by Boltzmann approximation:

$$n = N_c \cdot e^{\frac{-E_c - E_F}{kT}} \tag{2.1}$$

Where E_c is the energy at the bottom of the conduction band, N_c is the effective density of states near the bottom of the conduction band, E_F represents the Fermi level energy – degree of occupancy of the different energy states – and, lastly, kT represents the multiplication of the Boltzmann's constant by the temperature, in Kelvin.

On the other hand, for the valence band, the number of free holes, p, is given by equation (2.2), stating that:

$$p = N_v \cdot e^{\frac{-E_F - E_v}{kT}} \tag{2.2}$$

Considering that E_v is the energy at the top of the valence band and N_v is effective density of states in the valence band. Thus:

$$n = p = n_i \tag{2.3}$$

The excitation of electrons from the valence band to the conduction band originates the formation of free carriers. Therefore, to achieve the electroneutrality condition, the number of free electrons should be equal to the number of free holes. Hence, equation (2.4) shows that the Fermi level in an intrinsic semiconductor stays near the middle of the band gap [7].

$$E_F = E_i = \frac{E_c + E_v}{2} + \frac{kT}{2} \cdot ln\frac{N_v}{N_c} \tag{2.4}$$

When doped semiconductors are made, the band gap gets new energetic levels and the equality of number of free electrons and holes ceases to exist, but as a thermal equilibrium remains between charge carriers, equation (2.5) settles that:

$$n \cdot p = n_i^2 \tag{2.5}$$

In which n_i^2 is known as intrinsic concentration. This equilibrium inflicts the rearrangement of the position of the Fermi level, like so it leaves the surroundings of the middle of the gap, being moved either towards the conduction (n doping) or towards the valence band (p doping).

The agglutination of a donor and an acceptor, originates a p-n junction. When these are formed,

electrons create an electric field at the interface due to their transition from the n-type to the p-type semiconductor. Furthermore, this creates a depletion or space-charge region, where most of the impurities added are ionized – n part positively, p part negatively [9]. On this account, even if there isn't an applied external voltage, an electrostatic potential difference, V_b, given by equation (2.6), exists throughout the junction.

$$V_b = \frac{kT}{q} \cdot ln \frac{N_D \times N_A}{n_i^2} \tag{2.6}$$

Being N_D the density of positively charged donor ions, N_A the density of negatively charged acceptor ions and, lastly, $\frac{kT}{q}$ the thermal voltage, U_T, in which q is the electronic charge [10].

In the following subsections, topics related with solar cells and their operation are approached.

2.3.1 Representation of Solar Cells (Models)

For a better perception of solar cells, it is necessary to illustrate the 2 most frequently used models to represent them:

1. 1 diode and 3 parameters (1M3P);

2. 1 diode and 5 parameters (1M5P).

The first one serves as an ideal equivalent circuit, figure 2.1a, where the 3 parameters are the current generated by light, I_{PV}, the diode's reverse saturation current, I_S, and the diode's ideality factor, n. As it is an ideal model, it becomes unavoidable to represent the circuit as a more realistic case; in line with this, the 1M5P model, figure 2.1b, shows itself needful. The presence of electrical contacts and leakage currents are simulated by the series of a resistance, R_S, in parallel with another one, R_P. These are the 2 added parameters.

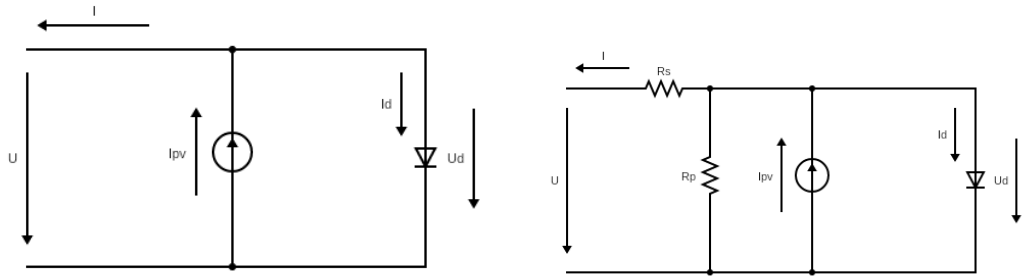

(a) 1M3P equivalent circuit. **(b)** 1M5P equivalent circuit.

Figure 2.1: Circuit representation of the two models that reproduce the operation of solar cells.

2.3.2 I–V Characteristic Curve

After a relatively brief insight into solar cells and their equivalent circuits representation, it is relevant to dive into their properties and operation. With this in mind, the I-V characteristic curve comes as a crucial thematic.

As it was formerly shown, a solar cell is known to behave like a diode, whose current flow, I_D, is given by:

$$I_D = I_S \left(e^{\frac{U_D}{n \cdot U_T}} - 1 \right) \tag{2.7}$$

Where U_D is the voltage applied across the diode. As a result, for the ideal case, the current flow in a cell, I_{cell}, is given by equation (2.8):

$$I_{\text{cell}} = I_{\text{PV}} - I_D \tag{2.8}$$

By equation (2.7) and (2.8), the final equation for the current flow in a solar cell is:

$$I_{\text{cell}} = I_{\text{PV}} - I_S \left(e^{\frac{U_D}{n \cdot U_T}} - 1 \right) \tag{2.9}$$

By simple inspection of the previous equation, it can be told that there is a relation of dependency between the current flow, I_{cell}, and the voltage across the diode, U_D. This relation is shown in figure 2.2. In this figure, the Maximum Power Point (MPP) is represented, also, allied with its respective axis, on the right. Other relevant points of this graphic are:

- I_{SC} – Short-circuit current. This is the point of maximum current that a solar cell achieves. It corresponds to $U_D = 0$;
- V_{OC} – Open-circuit voltage. Point of maximum voltage of a solar cell. Corresponds to $I_{\text{cell}} = 0$;
- I_{mpp} – Value corresponding to the current's coordinate of the maximum power point;
- V_{mpp} – Value corresponding to the voltage's coordinate of the maximum power point;
- P_{max} – Value of the power in the maximum power point.

From a theoretical point of view, it is possible to calculate the value of maximum power point from the I–V curve and P–V curve. For this calculation, equation (2.10) is needed, where C_0 is a constant dependent on the temperature of the solar cell, C_1 is the coefficient of temperature of I_{PV}, ΔT is the difference between the temperature of the cell and the room temperature and, finally, G_{ref} is the reference irradiance (1000 W/m^2).

$$I_{\text{PV}} = \left(C_0 + C_1 \frac{\Delta T}{G_{\text{ref}}} \right) \cdot G \tag{2.10}$$

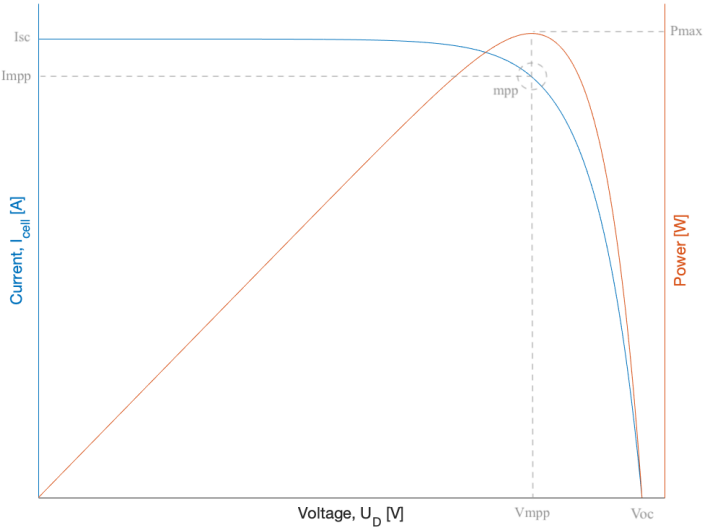

Figure 2.2: I–V characteristic curve of a solar cell.

The MPP is a point (*I,V*) that maximizes the area underneath the I–V curve. Therefore, the power of a solar cell and the maximum of its function is required. Given that:

$$P = U \times I = U_D \times I_{\text{cell}} = U_D \left(I_{\text{PV}} - I_S (e^{\frac{U_D}{n \cdot U_T}} - 1) \right) \tag{2.11}$$

And knowing $e^{\frac{U_D}{n \cdot U_T}} \gg 1$, it can be said that:

$$P \approx U_D \left(I_{\text{PV}} - I_S \cdot e^{\frac{U_D}{n \cdot U_T}} \right) \tag{2.12}$$

Then, by deriving the power in function of the voltage, equation (2.13), it is possible to calculate the MPP, since it is the point where the prior derivative is null.

$$\frac{dP}{dU_D} = 0 = I_{\text{PV}} - I_S \cdot e^{\frac{U_D}{n \cdot U_T}} \left(1 + \frac{U_D}{n \cdot U_T} \right) \tag{2.13}$$

Two other important equations to have in mind: the short-circuit current variation with irradiance, equation (2.14), and the open-circuit voltage variation with the relation $\frac{I_{\text{SC}}}{I_S}$, equation (2.15).

$$I_{\text{SC}} = I_{\text{SC}_{\text{ref}}} \cdot \frac{G}{G_{\text{ref}}} \tag{2.14}$$

$$V_{\text{OC}} = n \cdot U_T \cdot ln \left(\frac{I_{\text{SC}}}{I_S} + 1 \right) \tag{2.15}$$

Where $I_{\text{SC}_{\text{ref}}}$ is the reference short-circuit current [11].

2.3.3 Figures of Merit

Another relevant parameter when characterizing a solar cell is the Fill Factor (FF), that is given by equation (2.16). The FF demonstrates the similarity of the I-V curve behavior to a square shape. Furthermore, it also indicates (qualitatively) the performance of the device – it provides more power when closer to the unity.

$$FF = \frac{I_{\text{mpp}} \cdot V_{\text{mpp}}}{I_{\text{SC}} \cdot V_{\text{OC}}} \tag{2.16}$$

The aforementioned specifications are key points in the process of manufacturing and testing of solar cells, since they are crucial when dimensioning a solar PV system due to the power demand and other requirements of a specific installation. When calculating the power delivered by a system, it is important to have in mind that the groups of panels are dimensioned following two concepts:

1. For a number x of panels in series corresponds a voltage equivalent to $x \times V_{\text{OC}}$;

2. For a number y of panels in parallel corresponds a current equivalent to $y \times I_{\text{SC}}$.

Efficiency, η, is another key property of solar cells. Ultimately, this factor varies with the irradiance intensity, as it is shown is equation (2.17).

$$\eta = \frac{I_{\text{mpp}} \cdot V_{\text{mpp}}}{G \cdot A_{\text{cell}}} \tag{2.17}$$

Where G is the solar irradiance, in W/m^2, and A_{cell} is the area of the solar cell, in m^2 [12, 13].

2.3.4 Effect of Illumination and Temperature

The most determinant external factor in the operation of a solar cell is the amount of incident light. As it was formerly mentioned, it is usually measured by a coefficient known as irradiance (or flux density), that is a measure of power incident per unit area. Its respective units are W/m^2. Being an external factor, it varies depending on several aspects, such as the latitude, season and time of day at a given location. Furthermore, it is affected by other atmospheric conditions like clouds, dust or even relative humidity. Some of these will be considered in section Related Studies.

Besides what was previously stated, for a constant temperature, when the irradiance increases, it causes the value of currents to increase considerably, which means that the short-circuit current will be much higher. On the other, the open-circuit voltage has only a slight increase. This can be proved theoretically by inspection of equations (2.14) and (2.15). The referred relation is shown in figure 2.3.

For weak irradiances (30-50 W/m^2), polycrystalline (p-Si) solar cells present a significant drop in the open-circuit voltage, hence they should not be used in temperate countries. It is also known that silicon

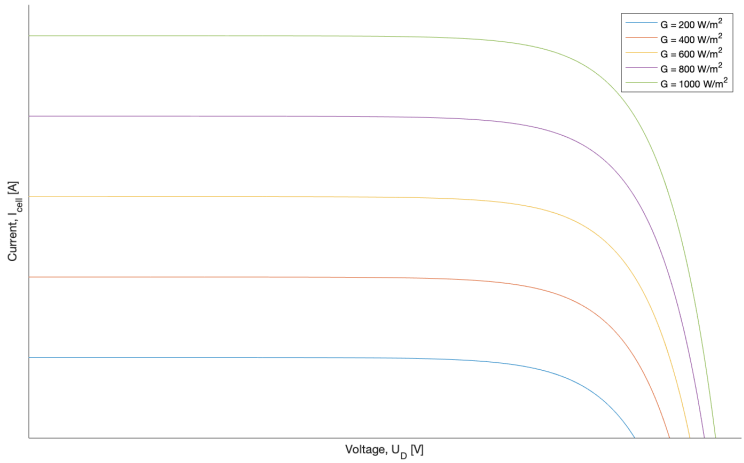

Figure 2.3: I–V characteristic curve for different values of irradiance.

solar cells are not sensitive to artificial light, but, in reduced illumination PV applications, amorphous silicon (a-Si) is known to operate notably due to its higher absorption coefficient.

In what concerns the variation of the curve for different values of temperature, for a constant irradiance, it can be noticed that I_{SC} remains approximately constant with an increase in the temperature, having an unnoticeable increase. Differently, the respective V_{OC} value decreases greatly with an increase of temperature. These phenomena are presented in figure 2.4. In silicon cells, the voltage decreases, typically, $2.2mV/^oC$ and expected total losses of around 15% at 60^o C [14].

The Standard Test Conditions (STC) for solar cells are $G = 1000\,\text{W/m}^2$, $T = 25°\text{C}$ and an airmass $AM = 1.5$.

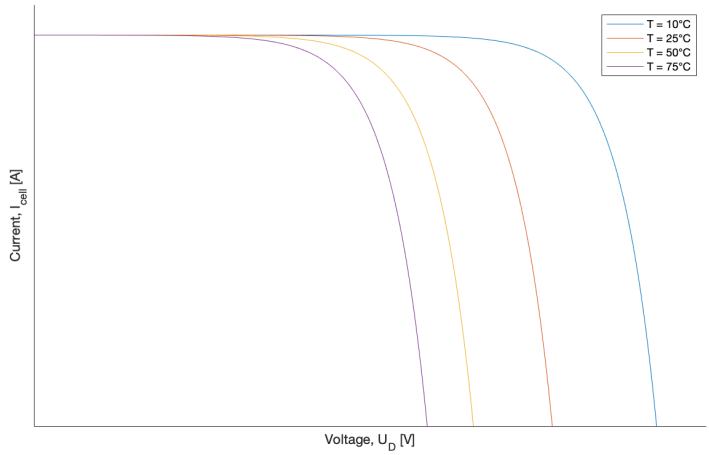

Figure 2.4: I–V characteristic curve for different values of temperature.

2.3.5 Bypass Diodes

Other very relevant factor affecting the efficiency of PV systems is the partial shading of cells, that reduces effectively the electrical energy generated by the solar cells. This occurs when a panel is not uniformly illuminated. Without bypass diodes, given a string of cells connected in series, the current of the string is limited to the worst performing cell. Thereafter, there is a decrease in power generation that implies the reduction of the effectiveness of the solar panel. Another problematic issue related to this behavior, is that limiting the current through the illuminated cells can result in higher voltages that can often reverse bias the worst performing cell, which may lead to huge power dissipation – hot-spot heating. This phenomenon often leads to destructive effects, such as cell or glass cracking, solder melting or to a degradation of the solar panel performance. In order to avoid this outcome, bypass diodes should be used in PV modules. The utilization of bypass diodes must obey a condition, given by equation (2.18): a single bypass diode bridges a certain number of cells, M, where V_C is the reverse breakdown voltage, V_F is the forward diode bias and V_{cell} is the illuminated cell voltage [12].

$$M \leq \left(1 - \frac{V_C + V_F}{V_{\text{cell}}}\right) \tag{2.18}$$

This method is implemented so that when the full shading of one cell occurs, inside a group of cells, the current of the illuminated groups is conducted by the bypass diode, avoiding the shaded one. In such a way, the current of the panel is not limited to the current of the worst performing group, although it produces a lower amount of electrical energy due to the non-operation of the total number of cells. In line with this, an ideal solution, from a conceptual perspective, would be to assign one diode to a single cell, increasing the power delivered by the panel due to the harnessing of every illuminated cell whether they are part of a group. This happens to be a non viable solution in the economic point of view and, for this reason, cells are grouped into sets in series, obeying to the condition above-mentioned.

2.3.6 Types of Solar Cells and Respective Generations

Solar cell technologies are constantly under study thus in continuous development; one evident fact that proves it is the division of solar cells in three generations already, sometimes four, although this last is not a widely accepted singular technology yet, but an improvement on the third one.

Each generation is classified depending on the raw material used upon the solar cell fabrication and on the level of commercial maturity and acceptance [15]. Each of them is also categorized due to their related efficiency and associated costs. This being the case, the three generations defined are characterized by:

1. Crystalline cells;

2. Thin films – three main families of components;

3. Nanocrystalline films, dye-sensitized, active quantum dots, organic-based cells and multi-junction cells – still under development and demonstration.

2.3.6.A First Generation

The first generation of solar cells is focused on PV technology based on thick crystalline films – mostly silicon-based – made by wafers of semiconductors. Silicon is used in both of its forms, forming monocrystalline (m-Si) and polycrystalline (p-Si) cells. The first ones have achieved efficiencies of the order of 24.4%, but the laters present a lower value, 19.9% [16], due to their lower material quality related to grain boundaries, defects and higher concentration of impurities. Silicon has the highest rate of usage for commercial solar cells, representing about 90% of the current PV market [17], since these cells have admirable conversion efficiency. Furthermore, the prior semiconductor is the second most abundant element on Earth, so the advantages of its availability in the future are a point to consider. Likewise, its chemical stability and non-toxicity are aspects that may enhance its lifetime as a cell material [15].

These first generation cells are also known to be based on gallium arsenide (GaAs), which achieves higher efficiencies, going for a range of 18.4-28.8% [16]. GaAs shows higher efficiency values, yet its cost of production makes it almost obsolete in comparison to other semiconductors and technologies. One of its main advantages is the broad spectrum of design options for PV cells applications that allows, for example, a more accurate control of the generation and collection of electrons and holes when compared to silicon cells, because these last ones have a limitation in the level of doping to achieve the same results [15].

2.3.6.B Second Generation

The second generation emerged as an attempt to reduce the high costs related to the first generation's manufacturing. It is based on thin film PV technologies, including three main ramifications:

1. amorphous silicon (a-Si) and micro amorphous silicon (a-Si/μc-Si);

2. cadmium telluride (CdTe);

3. copper indium selenide (CIS) and copper, indium gallium dieseline (CIGS).

In order to absorb the same amount of sunlight, thin-film solar cells need up to 99% less material than crystalline cells [18]. For this reason, combined with their known high flexibility, easy installation and diffuse light efficiency of about 12%, this type of solar cells is being more and more used in the last years [19]. However, thin-films' highest tested-in-laboratory value of efficiency is 20.3%, for CIGS [20],

10.2% and 12.7% for a-Si single-junction cells and multi-junction cells, respectively [16], and they present higher degradation than other types of cells .

When talking about single-junction cells, cadmium telluride is very relevant as it shows a band gap of 1.45 eV, known as an ideal gap, enhancing the conversion of sunlight into electricity, achieving a value of efficiency around 21% [16]. In relation to c-Si cells, cells made from CdTe do not have such a high (negative) impact on the output of the system when operating at higher temperatures and, in humid environments, they capture radiation better. Howbeit, beyond CdTe's materials are much scarcer than c-Si's, CdTe's toxicity and consequent potential environmental issues act as an obstacle upon its usability [17, 21].

Lastly, CIS and CIGS cells are formed by elements of groups I, III and VI of the periodic table, whose light absorption coefficients have high values and electrical characteristics that enable device tuning [22]. Nonetheless, these types of cells face major problems when it comes to degradation, as these materials' properties change under certain conditions. Adding to this factor, the scarcity of indium limits the low cost of manufacturing and the potential broadness of these technologies [23].

2.3.6.C Third Generation

This last generation arises with the aim of achieving high conversion efficiency devices using thin-film techniques in combination with low cost manufacturing – a mix between the main advantages of both previous generations. As Si-based cells, these last are made of non-toxic and abundant materials, thus their suitability for large-scale manufacturing and power generation [24]. Their high efficiency derives from nanostructured or organic materials, using several techniques, such as the hot carriers collection [25], the increase in the number of energy levels or even the generation of multiple carriers, known as impact ionization. Concerning these types of solar cells, processes like optimization of charge collection and enhancement of the energy captured within the solar spectrum are key points of study and betterment [26].

The utilization of organic PV cells seems very appealing due to several aspects: high flexibility and transparency, the possibility of being manufactured in a continuous printing process with a cost reduction, a wide area of coating and, as above-mentioned, their ecological benefits. Despite this, these cells still show some issues related to energy conversion, not achieving values as high as the first generation. In addition, their durability is somewhat limited due to the decomposition of the organic compound when electrons are excited to higher orbitals, resulting in anti-binding states [27].

With part-organic, part-inorganic, Dye-Sensitized Solar Cells (DSSC) belong to the category of hybrid solar cells, based on the mechanism of a fast regenerative photoelectrochemical process. When compared to traditional devices, these cells show a characteristic difference: the absorption of light is done by a functional element that is disassociated from the transport mechanism of the charge carriers,

which allows impure starting materials and simple cell processing, substantially reducing the cost of the device and resulting in conversion efficiencies of the order of 7-11% [28]. Through the last years, the improvement of this type of highly flexible and transparent cells has been a constant, already reaching efficiencies of 20% for semiconductors in the class of perovskite organometallic trialkyls, that can be used as light collecting components in DSSC. However, the stability over time and the effect of outdoor temperature range are a main issue regarding these dye-sensitized solar cells [17, 29].

To what nano-scale semiconductor materials belonging to groups II-VI, III-V or IV-VI of the periodic table are concerned, Quantum Dots Solar Cells (QDSC) have a discrete spectrum of quantized energy due to the confined movement of electrons and holes. By continuous research and development, although the estimated theoretical efficiency limit is 63%, these cells have achieved a conversion efficiency of around 11% [30, 31]. When talking about increasing this value, an issue emerges: diffusion of charge carriers, requiring new cell structures or the combination of these with other types of cells. The doping of QDSC with other materials allow an increase of the efficiency – with Si doping, a value of 17% can be obtained [15]. Some of their advantages consist on a favorable power to weight ratio, low power consumption and versatility, allowing their implementation not only on rooftops but on windows too.

Lastly, Multi-Junction Solar Cells (MJSC) – high efficiency cells, formed by multiple p-n junctions made of different semiconductor materials, each one producing electric current in response to different light wavelengths, thus taking advantage of the maximum number of photons possible. On the other hand, the higher the amount of junctions, the more complex the device will be, leading to expensive production costs [30]. That said, MJSC technologies are expected to surpass 50% of efficiency, presenting levels of 40% already [32]. Their high related costs make them economically infeasible for terrestrial applications, hence being preferred for spacial applications. Therefore, cost-effective, large-area and highly reproducible fabrication processes must be developed as a means to widen the use of multi-junction solar cells [17].

These third generation cells and respective aspects are still under experimentation and development, thus needing demonstration over recent researches and theories.

2.4 Related Studies

In this section, a chronological analysis of the chosen literature is shown in order to present relevant related studies to the work that is going to be shown thereafter. Several important research findings will serve as a foundation to the calculations carried out in the Experimental Results.

In 2003, Tamizhmani et al. [33], based on IEEE PAR 1479 "Recommended Practice for the Evaluation of Photovoltaic Module Energy Production", proposed a method to predict power/energy production as a function of ambient temperature, T_a, wind speed (W_{speed}), wind direction (W_{dir}), total irradiance and

relative humidity. They first developed a model based on the 5 inputs already mentioned, (2.19), and then tested another one based on 3 inputs only: ambient temperature, wind speed and global irradiance (2.20).

$$T_{\text{m}} = w1 \cdot T_{\text{a}} + w2 \cdot G + w3 \cdot W_{\text{speed}} + w4 \cdot W_{\text{dir}} + w5 \cdot \text{Humidity} + \text{const} \tag{2.19}$$

$$T_{\text{m}} = w1 \cdot T_{\text{a}} + w2 \cdot G + w3 \cdot W_{\text{speed}} + \text{const} \tag{2.20}$$

Where T_m is the temperature of the PV module and $w_x, x \in \{1, 2, 3, 4, 5\}$ are coefficients related to the different types of technologies and models used. These values can be checked in the original article [33].

They evaluated the two models by using a Neural Network from MATLAB Toolbox and explained that the 3 input model is more reliable due to lower related errors, as the errors in the measurement accuracy of wind direction and humidity may have a stronger influence than the two parameters themselves on the coefficient values; this phenomenon can be verified by their simulations, where several factors where compared, reaching a final conclusion: there is a simple linear relationship between the module temperature and the ambient conditions that can be simulated empirically by equation (2.21), where the respective units are °C for T_{a}, W/m^2 for irradiance and m/s for wind speed.

$$T_{\text{m}} = 0.943 \cdot T_{\text{a}} + 0.028 \cdot G - 1.528 \cdot W_{\text{speed}} + 4.3 \tag{2.21}$$

Where the w_x coefficients are replaced by average values processed by MATLAB's Neural Networks Toolbox, considering all the different technologies under study. This model, **Tamizhmani**, will be referred later, in chapter 3.

In 2011, Ruscheweyh et al. [34] approached the effect of wind loads on solar plants placed on rooftops. They stated that there are some parameters that influence wind loads, such as the angle of the module to the horizontal plane, the distance of the module rows to each other, the position of the module in the module field, the gaps between the module's respective gap to the ground, the supporting system and many others. One of their main concerns was a phenomenon called the leading edge vortex – when there is a wind flow directed towards the building corner.

In their research, they simulated the effect of wind in a wind tunnel by generating a wind profile by the Counihan Method, testing their model with a boundary layer for a free field, that is given by equation (2.22), being $W_{\text{speed}_{\text{ref}}}$ the wind speed at z_{ref}, that is the reference height and z the actual height. This approximation between wind speeds at different heights is valid assuming a laminar flow.

$$\frac{W_{\text{speed}}}{W_{\text{speed}_{\text{ref}}}} = \left(\frac{z}{z_{\text{ref}}}\right)^{0.16} \tag{2.22}$$

In addition to this, they also performed an analysis of the pressure distribution at the module, which is not homogeneous. Between a lot of concepts-description and further simulations, they came to the

conclusion that all the results had the same tendency once the modules at the rim of the module field present the maximum wind load. This last-mentioned is reduced gradually when moving towards the rear field, which shows a significantly reduced load, due to the wind shadow effect [34].

Still in 2011, Jiang et al. [35] studied the influence of meteorological parameters on photovoltaic modules in some cities in the Niger Delta of Nigeria. Some of the main factors that affected the results were the cloud cover, solar flux and relative humidity. That said, in order to test the same inputs at different locations, they performed the same type of experiments in Bori town and Port Harcourt city.

Thereafter, by computing the graphs of solar flux, relative humidity, time of the day, solar panel temperature and relative humidity against efficiency, they were able to conclude that low relative humidity (65%-73%) corresponds to a relative efficiency of 96% and if the solar panel temperature increased above 45°C, the output current would drop, reducing efficiency. Accordingly, Port Harcourt, being a more industrialized and densely populated city, presents a lower efficiency due to emissions from industries and motorized vehicles, masking and preventing solar flux from reaching the solar panel with that much intensity. Bori, located far from the sea shore thus shrouded with lower relative humidity, showed a higher output current, hence an higher conversion efficiency [35].

Later, in 2013, Veldhuis et al. [36] investigated the influence of wind on the temperature of PV modules in tropical environments by comparing three predictive models for different PV technologies (p-Si, m-Si, hetero-junction Si, a-Si). The first one is the widely known Ross model [37], given by equation (2.23), being k the Ross coefficient, which relates the incident irradiance on the module plane, G_m, to the temperature increment.

$$T_m = T_a + kG_m \tag{2.23}$$

The second model, a simple semi-empirical correlation, was proposed by Skoplaki et al. [38] being the first model to include the wind speed, as shown in equation (2.24).

$$T_m = T_a + \omega \left(\frac{0.32}{8.91 + 2.0 W_{\text{speed}}} \right) \tag{2.24}$$

In which ω is the mounting coefficient – ratio related to the Ross coefficient for the mounting situation and the Ross coefficient for a well-ventilated, free-standing system.

Ultimately, a model proposed by King et al. [39], also taking wind into account, given by equation (2.25), where *a* and *b* are empirical coefficients and V_w is the wind speed at 10 m height.

$$T_m = G_m \cdot \left(e^{a+b \cdot V_w} \right) + T_a \tag{2.25}$$

Due to various heights of the PV environment under study, they approximated the differences in wind speeds by the power law profile (2.22), as used by Ruscheweyh et al., but using n as the exponential,

given by equation (2.26), instead of 0.16.

$$n = \frac{0.37 - 0.0881 \cdot ln(W_{speed_{\text{ref}}})}{1 - 0.0881 \cdot ln\left(\frac{z_{\text{ref}}}{10}\right)} \tag{2.26}$$

After computing the simulated versus experimental results, they ended up by noticing that the deviations increased with rising temperatures and that the results of the Ross model showed significantly large errors for higher PV module temperatures. Furthermore, they identified that depending on the PV module technology and location, the three models produced approximately the same results with a root mean square error between 1.5-3.8°C, corresponding to a deviation in power output between $0.3 - 1.6\%$. Nevertheless, they state the Skoplaki and King models correlate slightly better and the main issue of the Ross model is the struggle to select the appropriate Ross coefficient, which can affect the accuracy considerably.

In this very same year, Schwingshackl et al. [40] performed a work of such a great value in what concerns the models used in the calculations of this dissertation, as it will be reflected in Experimental Results. In order to compare the accuracy of the different models that include and do not include wind data to predict PV cell temperature, assuming that the temperature of the model is the same as the cells' [41], they studied the cooling effect of wind on PV cell temperature for different cell technologies installed at a PV test facility in Bolzano, Italy, taking into consideration the module temperature as a function of solar irradiance, ambient temperature and wind, as shown in the prediction models below. Schwingshackl et al. performed in-situ measurements, using sensors installed at a weather station placed next to the PV plant for obtaining the meteorological parameters. The PV cells temperature was recorded at the back of the modules. In addition to these measurements, they also used wind data from the European Centre for Medium-Range Weather Forecasts (ECMWF).

Regarding the cell temperature prediction, eight models were used. The ones introduced here are the models pertinent to the work developed in this thesis – these will be used in Methodologies and Experimental Results. As a consequence of their importance, their names are displayed in bold. All of these models relate the cells (therefore, the module) temperature with the incoming irradiance and relevant meteorological parameters.

The first model is the so called SA (2.27), in which the cell temperature is given by:

$$T_c = T_a + \frac{G}{G_{\text{NOCT}}} \cdot (T_{\text{NOCT}} - T_{\text{a,NOCT}}) \tag{2.27}$$

Where G is the in-plane irradiance, T_{NOCT} is the nominal operating cell temperature, a factor whose value depends on the PV technology, as it will be explained in chapter 3. G_{NOCT} and $T_{\text{a,NOCT}}$ are parameterized values: 800 W/m^2 and 20°C, respectively. Although the full description of Nominal Operating Cell Temperature (NOCT) can be found in [42], it is important to know that it considers a wind speed of

1 m/s.

The **SA** was the reference model used by Schwingshackl et al. and it is the model that will be used later as a reference when performing comparisons.

The second and third models are advanced models proposed by Skoplaki et al. [43], here called **Skoplaki 1** and **Skoplaki 2**, respectively. As follows, they take wind data into account and both of them rely on (2.28).

$$T_c = T_a + \frac{G}{G_{\text{NOCT}}} \cdot (T_{\text{NOCT}} - T_{\text{a,NOCT}}) \cdot \frac{h_{\text{w,NOCT}}}{h_w} \cdot \left[1 - \frac{\eta_{\text{STC}}}{\tau \cdot \alpha}(1 - \beta_{\text{STC}} T_{\text{STC}})\right] \tag{2.28}$$

Being h_w the wind convection coefficient, $h_{w,\text{NOCT}}$ the wind convection coefficient at NOCT conditions (where $W_{\text{speed}} = 1$m/s), η_{STC} is the efficiency of the module at STC, τ is the transmittance and α is the absorptance – their product is assumed to be equal to 0.9 [44] –, β_{STC} is the temperature coefficient of maximum power of the module and T_{STC} is the temperature at STC conditions, 25°C.

What differs between the two last-mentioned models is the parameterization of $h_w(v)$. Skoplaki 1 uses the parameterization developed by Skoplaki et al., as demonstrated by (2.29) and Skoplaki 2 refers to the parameterization suggested by Armstrong et al. [45], given by (2.30).

$$h_w = 5.7 + 2.8 W_{\text{speed}} \tag{2.29}$$

$$h_w = 8.3 + 2.2 W_{\text{speed}} \tag{2.30}$$

The wind speed is the local wind speed measured close to the module.

The fourth model was developed by Koehl et al. [46], but makes use of an empirical model advanced by Faimann [47]. In this way, Koehl et al. specify the values of the U_0 and U_1 constants for different PV cell technologies, which are used in (2.31) – equation that describes the **Koehl** model.

$$T_c = T_a + \frac{G}{U_0 + U_1 \cdot W_{\text{speed}}} \tag{2.31}$$

In an attempt to suggest an evolved prediction model, Mattei et al. [48] proposed one that says the PV cell temperature follows the subsequent equation, (2.32):

$$T_c = \frac{U_{\text{PV}} T_a + G \cdot [\tau \cdot \alpha - \eta_{\text{STC}}(1 - \beta_{\text{STC}} T_{\text{STC}})]}{U_{\text{PV}} + \beta_{\text{STC}} \cdot \eta_{\text{STC}} \cdot G} \tag{2.32}$$

Where U_{PV} is the heat exchange coefficient for the face of the module. Since they refer two possible parameterizations for this variable, this implies the existence of two models: **Mattei 1** and **Mattei 2**, following the procedure described for the Skoplaki models. In the first one (2.33), U_{PV} is reported such

as:

$$U_{\text{PV}} = 26.6 + 2.3W_{\text{speed}} \tag{2.33}$$

In Mattei 2 (2.34), it is given as:

$$U_{\text{PV}} = 24.1 + 2.9W_{\text{speed}} \tag{2.34}$$

Similarly to (2.29) and (2.30), W_{speed} is the wind speed measured close to the module.

Finally, a model proposed by Kurtz et al. [49] that does not consider parameters associated with each PV technology. This being said, the **Kurtz** model (2.35) proposes a correlation between cell temperature, ambient temperature, irradiance and wind speed given by:

$$T_c = T_a + G \cdot e^{-3.473-0.0594W_{\text{speed}}} \tag{2.35}$$

Likewise the previous models, this one includes the local wind speed as a variable.

In this study, Schwingshackl et al. compared the temperature measured at the bottom of the PV modules with the values given by the prediction models, as said above, for several time steps. With this, they separated their work into two: data from in-situ measurements and data from the European Centre for Medium range Weather Forecast (ECMWF). After acquiring all the data required, they calculated the coefficient of determination (R^2) and the Root Minimum Squared Error (RMSE) between both sources of data and the actual temperature measurements in order to get a quantitative indication of each model's performance – the best model is the one that maximizes R^2 and minimizes the RMSE. With this, they reached some appropriate results. Schwingshackl et al. state that for p-Si cells, models Mattei 1 and Mattei 2 are the most accurate. When it comes to CdTe, they report that the SA and Kurtz model achieve the best results, indicating that it happens "probably because those PV modules have a higher thermal inertia than the silicon PV technologies" [40, p. 6].

Having said that, they make it pretty clear that since all PV technologies have different characteristics thus different behaviors, when estimating the temperature of the modules (taking wind data into account), it would be fallacious to select a generalized approach.

In 2014, Bhattacharya et al. [50] calculated the effects of ambient temperature and wind speed on the performance of monocrystalline solar PV modules after almost 1 year of data collection, to cover seasonal influences. The aim of the study was to find the variation of efficiency with the 2 preceding parameters.

The calculation of the correlation coefficient, R was done considering ambient temperature and wind speed as independent variables and efficiency as dependent variable separately. Herewith, their research suggests the following relations between ambient temperature and efficiency (2.36) and between

wind speed and efficiency (2.37), in the stated order:

$$\eta = 8.6621 + 0.1355 \cdot T_a, R^2 = 92.97\% \tag{2.36}$$

$$\eta = 11.8218 + 0.4172 \cdot W_{\text{speed}}, R^2 = 47.02\% \tag{2.37}$$

Considering a confidence level of 95%. These results confirmed a strong positive correlation between ambient temperature and efficiency. On the other hand, in what the correlation between wind speed and efficiency is concerned, only a moderate positive linear relationship was confirmed. In closing, Bhattacharya et al. suggest that the differences verified for the power output regarding different module's orientations may be related to the deviation from the STC. As a result, they stated that when designing green buildings, besides considering only the orientation of the solar PV modules, the ambient parameters should also be taken into consideration [50].

By the year of 2016, Kilikevicius et al. [51] performed an analysis of external dynamic loads influence to PV module structural performance, triggered by the factor that the efficiency of modern PV systems decrease when the crystalline structure of the modules is damaged due to climatic factors, such as wind and similar dynamic effects and that general IEC certifications for PV modules (IEC 61215, IEC 61646) consist of only static tests, although they operate in dynamic environments thus subject to dynamic factors.

They emphasize the importance of wind on efficiency as, from the fluid engineering point of view, inclined PV modules are a barrier against the airflow. They also indicate that turbulence effects in incident flow (plus above and below the module) could change the flow and the occurring forces, hence affecting the operation of the module, given that turbulence and stall can cause their periodic excitation.

Kilikevicius et al. also refer that movement and oscillations are led by varying pressure difference between the two module sides, which implies that the mounting system and the PV modules have to stand the occurring forces already mentioned. These factors are main issues when thinking about durability, maintenance and efficiency of the entire PV system. Hereby, they mention a paper where Weiss et al. [52] presented the correlation between the pressure, P, onto the module and the deflection, m_d of the module in the range between -10 and +10 mm, given by equation (2.38), considered to be very useful for the design of indoor test-facilities for dynamic mechanical loads.

$$P = -62.689 m_d - 0.21895 m_d^2 - 0.1127 m_d^3 \tag{2.38}$$

The aim of this work was to investigate the feasibility of acquiring modal parameters of a damage structural element by using operational modal analysis, for purpose of condition assessment. Thereupon, they proceeded to load the PV module with external excitation in the frequency of 0 to 40 Hz as a means to simulate the dynamic mechanical loads by changing the vibration's amplitude magnitude and

frequency – matching different wind speeds.

After all things considered, a mismatch between theoretical results and experimental modal analysis results varying from 0.74% to 7.40% was obtained and, furthermore, it was found that low-frequency vibrations can cause considerable damage to the PV modules, particularly when it reached the FE model resonant frequency at 16 Hz. By the end of the experiment, some crystalline structures of the PV module unveiled cracks, which can be a crucial issue causing a lower light input and energy flow failures. In the worst case, the outcome can be the total failure of the PV module [51].

Also in 2016, Amajama et al. [53] studied the impact of wind on the output of a photovoltaic panel (mono-crystalline cell type), experimentally. The results were analyzed by computing the output current and the output voltage versus wind speed at nearly constant air temperature, air pressure, relative humidity and solar illuminance/intensity. Along with that, it was tested the relation between wind speed and solar illumination/intensity, maintaining also the aforesaid parameters nearly constant. That being said, they state that wind speed, having an effect on radio waves propagation, aids it if the wind is flowing in parallel to the signal, but acts in the adverse way if it is tangential or anti-parallel, impairing the propagation of the radio waves. Moreover, they pointed out the similarity between these waves and electromagnetic radiations, that share comparable properties.

With the formerly mentioned in mind and following the data analysis, they attained two advantageous (A, B) and two disadvantageous (C, D) situations, respecting the performance of the PV module in function of the wind: (A) when wind is towards the front of an observer (or panel) with the sun some distance away in front; (B) when wind is towards the back of the observer (or panel) and the sun is behind; (C) when wind's direction is towards the back of an observer (or panel) and the sun is some distance in front of the observer (or panel); (D) when the sun is some distance behind the observer (or panel) and the wind direction is towards the front of the observer (or panel).

To sum up, in this last study, it was evidenced that, under the same conditions, when the molecular particles of the wind are in phase with the direction of the solar photonic particles, solar illuminance/intensity is favoured, thus unfavoured when out of phase. Consequently, the same phenomenon occurs in relation to the output of a photovoltaic panel [53].

In this chapter, State of the Art, various concepts were introduced in order to support the work that is going to be presented afterwards. Firstly, a brief introduction and contextualization of the solar photovoltaic technology was given and the most important factors in the operation of solar cells were explained. Then, some of the diverse PV technologies were summarily described. Lastly, it was analyzed some opportune literature, whose value lies on the general comprehension of the topic and its possible branches.

3

Methodologies

Contents

In this third chapter, as the title suggests, it will be given the definitions of the methodologies to be used, i.e., by what means the thematic introduced in chapter 1 is going to be developed. Between all the new-era softwares and available information, a major concern relies on how to gather trusted sources and achieve tangible and authentic results by simulation methods and calculations.

3.1 Theoretical Foundations

The operation and characteristics of solar cells, exhibited in State of the Art, work as a starting and a finishing point to this study, owing to the fact that wind is known to have an influence in PV systems, as shown in Related Studies. Accordingly, following the equations that represent the operation of solar cells, it is imperative to know how wind and its mutable characteristics affect each of them and to know its effect on the overall performance of the system. The behavior mentioned can be affected directly – for example, by the temperature of cells – or indirectly – by magnetic interference between cables and consequent change in current characteristics.

With the previously mentioned in mind, the equations already explained serve as a foundation to all of the remaining work.

3.2 Cell Temperature Prediction Models

As this dissertation is focused on the effect of wind velocity and wind shadowing on energy generation of solar plants – by studying the changes in temperature of solar cells according to the technologies and designs used –, the temperature values of the different modules must be known. Having said that, the tools that will allow the acquisition of those values are the cell temperature prediction models mentioned in the previous chapter, which are summarized in table 3.1.

As pointed out before, the reference model is the Standard Approach. Although the NOCT formula implies a wind speed of 1 m/s, it doesn't take accurate wind data into account – despite wind's known volatility – and, notwithstanding its flaws, it is an industry standard method for calculating cells' temperature. Therefore, it becomes mandatory to cement fundamental notions when forecasting the power variation due to wind loads by consequent cell temperature fluctuations in solar plants.

With this, temperature and resultant power deviations between all the models suggested will be analyzed in order to understand how different PV technologies behave upon different prediction models and different wind speeds. This work will be applied to all the modules present in the geometry detailed in Computational Fluid Dynamics so as to investigate the effect of wind shadowing between PV arrays.

Table 3.1: List of cell temperature prediction models.

Model	Formula
Standard	$T_c = T_a + \frac{G}{G_{\text{NOCT}}} \cdot (T_{\text{NOCT}} - T_{\text{a,NOCT}})$
Skoplaki 1	$T_c = T_a + \frac{G}{G_{\text{NOCT}}} \cdot (T_{\text{NOCT}} - T_{\text{a,NOCT}}) \cdot \frac{h_{\text{w,NOCT}}}{h_w} \cdot \left[1 - \frac{\eta_{\text{STC}}}{\tau \cdot \alpha}(1 - \beta_{\text{STC}} T_{\text{STC}})\right], h_w = 5.7 + 2.8 W_{\text{speed}}$
Skoplaki 2	$T_c = T_a + \frac{G}{G_{\text{NOCT}}} \cdot (T_{\text{NOCT}} - T_{\text{a,NOCT}}) \cdot \frac{h_{\text{w,NOCT}}}{h_w} \cdot \left[1 - \frac{\eta_{\text{STC}}}{\tau \cdot \alpha}(1 - \beta_{\text{STC}} T_{\text{STC}})\right], h_w = 8.3 + 2.2 W_{\text{speed}}$
Koehl	$T_c = T_a + \frac{G}{U_0 + U_1 \cdot W_{\text{speed}}}$
Mattei 1	$T_c = \frac{U_{\text{PV}} T_a + G \cdot [\tau \cdot \alpha - \eta_{\text{STC}}(1 - \beta_{\text{STC}} T_{\text{STC}})]}{U_{\text{PV}} + \beta_{\text{STC}} \cdot \eta_{\text{STC}} \cdot G}, U_{\text{PV}} = 26.6 + 2.3 W_{\text{speed}}$
Mattei 2	$T_c = \frac{U_{\text{PV}} T_a + G \cdot [\tau \cdot \alpha - \eta_{\text{STC}}(1 - \beta_{\text{STC}} T_{\text{STC}})]}{U_{\text{PV}} + \beta_{\text{STC}} \cdot \eta_{\text{STC}} \cdot G}, U_{\text{PV}} = 24.1 + 2.9 W_{\text{speed}}$
Kurtz	$T_c = T_a + G \cdot e^{-3.473 - 0.0594 W_{\text{speed}}}$
Tamizhmani	$T_c = 0.943 \cdot T_a + 0.028 \cdot G - 1.528 \cdot W_{\text{speed}} + 4.3$

3.3 Software Manipulation

In order to perform complex engineering computations, a model of each of the intended PV geometries had to be created by scratch. For this task, a Computer-Aided Design (CAD) software is needed and the chosen softwares were FreeCAD – an open-source parametric 3D modeler that allows the user to design real-life objects – and Fusion 360 – a more complex tool, with the aim of 3D modeling to design and product manufacture, used here under an educational license. The first one was used to create the solar PV geometries and the later-mentioned ensured the design of the wind tunnels.

When it comes to Computational Fluid Dynamics (CFD), which is "a science that, with the help of digital computers, produces quantitative predictions of fluid-flow phenomena based on the conservation laws (conservation of mass, momentum, and energy) governing fluid motion" [54, p. 421], the software that allowed its concretion was Autodesk CFD – a CFD simulation software that engineers can use to predict how liquids and gases will perform when applied to some CAD geometry. Autodesk CFD offers a wide range of possibilities in what concerns the needed parameters, i.e. the wind speeds for the several modules that constitute the sets of PV arrays, as it will be described in Computational Fluid Dynamics.

Once acquired the wind speed values by means of CFD, Microsoft Excel was the designated software to compute the calculations of the temperature (and associated peak power variation) for every single module, according to each 1) model, 2) solar cell technology and 3) wind speed value.

3.4 Reference Data

As this investigation intends to propose a general perspective on how wind affects the performance of solar plants, it is required that the CFD simulations are based on suitable and concrete data, such as realistic atmospheric conditions and characteristic values, for instance, the parameters of solar cells, dimensions of the PV modules and the support system designs. In the following subsections, all of the values regarding these characteristics will be unveiled.

3.4.1 Wind

In what concerns wind speeds, as there are multiple sources of meteorological information, it will be taken into account data made available by Instituto Português do Mar e da Atmosfera (IPMA) and Meteored. The standard values for wind are classified as following:

1. The direction of wind is given by only 8 paths: N, NE, E, SE, S, SW, W, NW;
2. The intensity of wind, for general purposes, is expressed (in terms of average intensity per 10 minutes) by:
   (a) Light wind $<$ 15 km/h ($\approx$ 4.167 m/s);
   (b) 15 km/h $<$ Moderate wind $\leq$ 35 km/h ($\approx$ 9.722 m/s);
   (c) 36 km/h ($\approx$ 10 m/s) $<$ Strong wind $\leq$ 55 km/h ($\approx$ 15.278 m/s);
   (d) 56 km/h ($\approx$ 15.556 m/s) $<$ Very strong wind $\leq$ 75 km/h ($\approx$ 20.883 m/s);
   (e) Exceptionally strong wind $>$ 75 km/h.

Having in mind that wind speed is given by multiples of 5 km/h, for general purposes [55].

As for simulating a real-life approach, concrete wind speed data was collected. Table 3.2 shows the maximum and average wind speed values for the Lisbon district throughout the year 2020, where W_{max_1} and W_{avg_1} are collected from Meteored [56] and W_{max_2} from IPMA [57]. Unfortunately, IPMA doesn't provide info on the values of average wind speed for each month on their Monthly Climate Bulletin; that is the reason why these values aren't shown in the table below.

By inspection of table 3.2, it is possible to notice that the average values of W_{max_1} and W_{max_2} are very similar. Due to coherence, the value that will be used is the first one, once IPMA doesn't provide the average values for wind speed.

To be used in chapter 4:

- W_{max} = 17.55 m/s – Average Maximum Wind Speed;
- W_{avg} = 4.06 m/s – Average Average Wind Speed.

Table 3.2: Maximum and average wind speeds for Lisbon in 2020.

	W_{max_1} (m/s)	W_{max_2} (m/s)	W_{avg_1} (m/s)
January	19.67	18.11	4.02
February	16.09	14.81	3.13
March	19.67	20.69	4.47
April	17.43	17.31	4.02
May	16.54	17.69	4.02
June	16.09	14.69	4.47
July	17.88	14.61	4.92
August	18.33	18.50	4.92
September	17.88	18.31	4.02
October	17.43	15.50	4.02
November	17.43	15.31	3.13
December	16.09	22.00	3.58
AVERAGE	**17.55**	**17.29**	**4.06**

3.4.2 Ambient Temperature and Irradiance

As it can be seen in Cell Temperature Prediction Models, all models consider T_a and G – ambient temperature and irradiance, respectively. Having noticed that, it is crucial to use suitable data so that one may reach appropriate results.

Knowing that NOCT conditions require $G_{\text{NOCT}} = 800\,\text{W/m}^2$ and $T_{a,\text{NOCT}} = 20\,^{\circ}\text{C}$, the values chosen for the in-plane irradiance and ambient temperature are the same as the NOCT ones so that $G = G_{\text{NOCT}} = 800\,\text{W/m}^2$ and $T_a = T_{a,\text{NOCT}} = 20\,^{\circ}\text{C}$. Beyond wind speed values, the remaining variables depend on the PV technologies used, as showcased in the forthcoming subsection.

3.4.3 PV Technologies

Given that there are many PV cells technologies, it is imperative to simulate the most convenient ones. With this purpose, p-Si, CdTe and CIGS technologies were the ones selected. Being that different technologies behave differently due to their intrinsic characteristics and, as beforesaid, aiming to the most accurate real-life simulation results, three distinct solar panels datasheets were collected – one for each technology. These datasheets can be found in [58], [59] and [60], by the order mentioned above, respectively.

This being said, table 3.3 presents a synthesis of the main characteristics of the chosen PV modules at Standard Test Conditions, obviously except for the last row.

Table 3.3: Main parameters for each solar cell technology.

		Technology		
Parameter		p-Si	CdTe	CIGS
Dimensions (mm)	L×W×T[1]	1645×992×35	1200×600×6.8	1257×977×35
Nominal Power (W)	P_{mpp}	255	122.5	170
Voltage at P_{max} (V)	V_{mpp}	30.40	71.5	87.5
Current at P_{max} (A)	I_{mpp}	8.39	1.71	1.95
Open Circuit Voltage (V)	V_{OC}	38.07	88.7	112
Short Circuit Current (A)	I_{SC}	8.89	1.85	2.20
Efficiency (%)	η	15.6	17.0	13.9
Temperature Coef. of P_{mpp} (%/°C)	β_{STC}	-0.39	-0.28	-0.31
NOCT (°C)	T_{NOCT}	45	45	47

[1] *Length x Width x Thickness*

Remembering that the cell temperature prediction model proposed by Koehl et al. requires coefficients U_0 and U_1 that are dependent on the PV technology used, table 3.4 sums their corresponding values.

Table 3.4: Coefficients for the Koehl model.

	Technology		
Coefficient	p-Si	CdTe	CIGS
U_0	30.02	23.37	22.19
U_1	6.28	5.44	4.09

Chapter 3 compiles the most essential data for the chapters that follow. Hereby, it can function as an introduction to the work that is yet to be showcased and it can work as a returning point, if necessary. It includes all the cell temperature prediction models to be used, decisive weather data and all the relevant information on the photovoltaic technologies that are part of this study.

4

Computational Fluid Dynamics

Contents

Computational Fluid Dynamics is a branch of fluid mechanics that allows the study of fluid flows using numerical solution methods. It consists of three main stages:

- Pre-processing;
- Processing;
- Post-processing.

The first stage of a CFD study involves the problem analysis – understanding the problems that one needs to solve and setting objectives –, which has been done already. It also deals with CAD modeling, meshing and the solver setup. The second stage has simulations and their validation as its focus; pre-processing plays a critical role on this step because it determines either a smooth simulation (when done correctly) or it can prevent the simulations from running (when done incorrectly). The final stage is related to the analysis of the results obtained – using the tools available with the aim of achieving the most accurate reports or graphical representations of the results. This step will be part of chapter 5.

Before proceeding to the computational simulations, a CAD geometry of the PV arrays had to be created having in mind its real dimensions. The steps underlying this process are detailed in the next sections, as well as various computational fluid dynamics stages and requirements, such as, for instance, wind tunnel sizing and the turbulence model used in order to simulate wind behavior, just like their fundamentals.

4.1 Solar Photovoltaic Modules

As it was already mentioned, for the purpose of reaching veracious results through simulation methods, photovoltaic arrays sizing has to be in conformity with reality. Hereby, their CAD dimensions must be the same as specified in the respective datasheet and the distance between rows should be appropriate thus reflecting a concrete scenario.

4.1.1 Dimensions

Once each company produces PV modules of distinct sizes, it wouldn't be adequate to simulate different geometries and then compare the results obtained, given that the design of each structure influences the aerodynamics hence the wind speeds around solar panels. Knowing that the aim of this study is to investigate how wind speeds around photovoltaic arrays may affect their temperature and consequent output power variation, it would lead to misleading results. For this reason, only one geometry was considered, having in mind that the Temperature Coefficient of P_{mpp} and the remaining parameters accounted in every cell temperature prediction model are technology/material-specific and their value

isn't dictated by module's dimension. This being said, from now on, it is assumed that the dimensions of each PV module are the same, apart from the technology.

Herewith, the geometry selected corresponds to the p-Si technology [58] – by table 3.3, it can be verified that its dimensions are 1645 x 992 x 35 mm. This design and all its parts (yet to be shown) were built via FreeCAD. This single PV module can be observed in figure 4.1. After creating the reference solar module, the process of replicating it is quite straightforward.

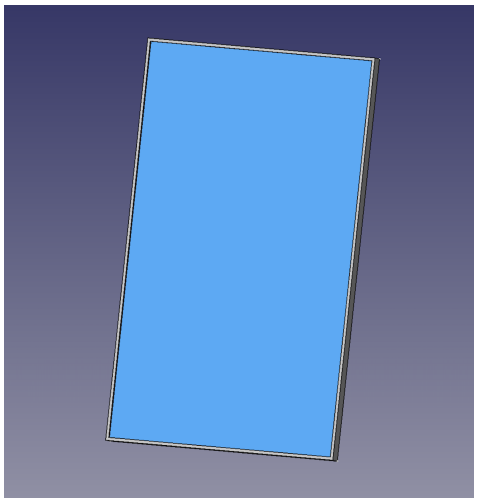

Figure 4.1: Single solar panel.

The next step was to create the support structure. To perform this task, it must be foreknown that a standard inclination for PV panels in Portugal is 30°. Figure 4.2 displays the support structure sized to fit three modules distancing 100 mm from each other, being that the only module present is the central one – in grey.

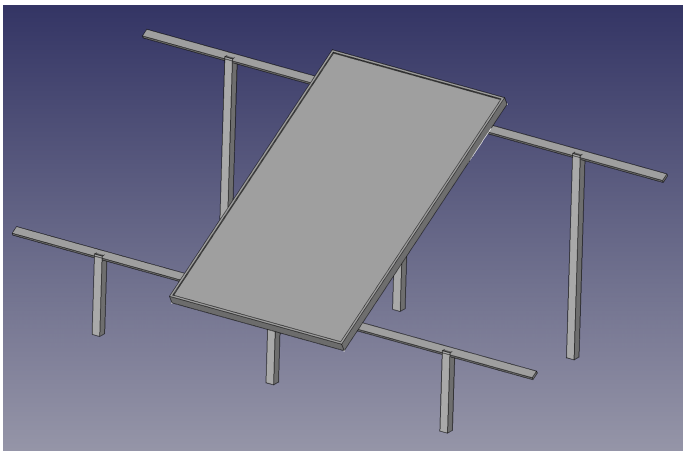

Figure 4.2: Single solar panel on support structure.

As soon as the structure is created, the phase that follows is the simple replication of the panel to

the top of the mounting structure, as it can be noticed in figure 4.3 – blue panels. Its rear view is shown in figure 4.4. At this time, the reference array – mounting system with three panels – is created, leaving only simple tasks to be performed: creating clones of the reference array and changing their location in space.

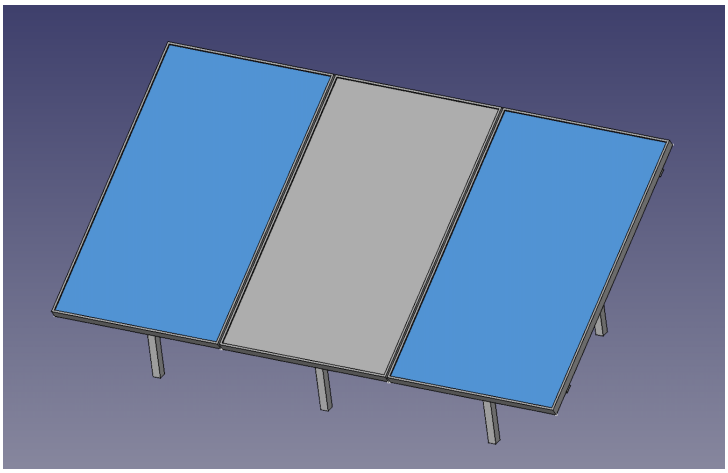

Figure 4.3: Reference array of three PV modules.

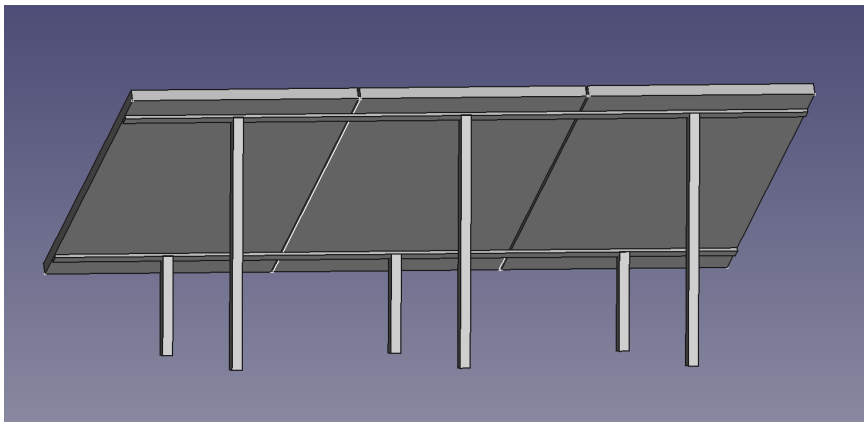

Figure 4.4: Reference array of three PV modules – rear view.

In order to create clones of the reference array, one measure has to be taken into account: distance between front and back rows of panels. This is detailed in the following subsection.

4.1.2 Distance Between Rows

Distance between rows of arrays is of utmost importance due to the fact that a partially shaded solar panel has its output power reduced or, in the worst case, completely nullified, as mentioned in Bypass Diodes. The avoidance of this scenario is done by increasing distance between rows. Nevertheless, an optimization of array spacing can turn into a really complex task – adding the fact that it is location/site-

dependent. Hence, it was decided that this sizing would be executed via a mix between a common simplification method – considering the winter *solstice* – and an adaptation of this same method, since it is the worst possible case and implies a lot of space between rows of photovoltaic arrays. *Solstice* means the ”the sun stands still”. When this phenomenon occurs, the noonday Sun is at its minimum altitude and this is the smallest day of the year for latitudes above 23.5° N (for the Northern hemisphere) [61] – the case of Lisbon, whose latitude is around 38.64° N [62]. The determined method respects equation (4.1), where d is the inter row spacing, L is the module length, θ its inclination and ω is the solar radiation angle [63].

$$d = L \cdot \left(cos(\theta) + \frac{sin(\theta)}{tg(\omega)} \right) \tag{4.1}$$

In 2020, Lisbon's winter solstice was in the 21st of December and the sun reached a minimum height of 28° upon its meridian passage [64], which is the value of ω. Remembering that the PV panels have a tilt angle of 30° and knowing that the total length of the module is 1645 mm, this would require a gap of about 3 m, which sometimes is not feasible owing to land limitations. As it is known that sunlight incidence on solar panels depends on the movement of the sun - a factor ignored by this method –, the maximum heights of the sun for a timestep of ten days throughout the year of 2020 (3 dates per month, 36 in total) were analyzed. Their average value was around 54° [65]. Since these are the maximum heights, it wouldn't be as correct to scale the distances having this value as a reference. It was decided that a suitable value would be 54° - 5° = 49°, which implies an inter row spacing between solar panels equal to 2140 mm.

Having this distance estimated, it was possible to progress to the next stage: replication of the reference array, as seen in figure 4.5.

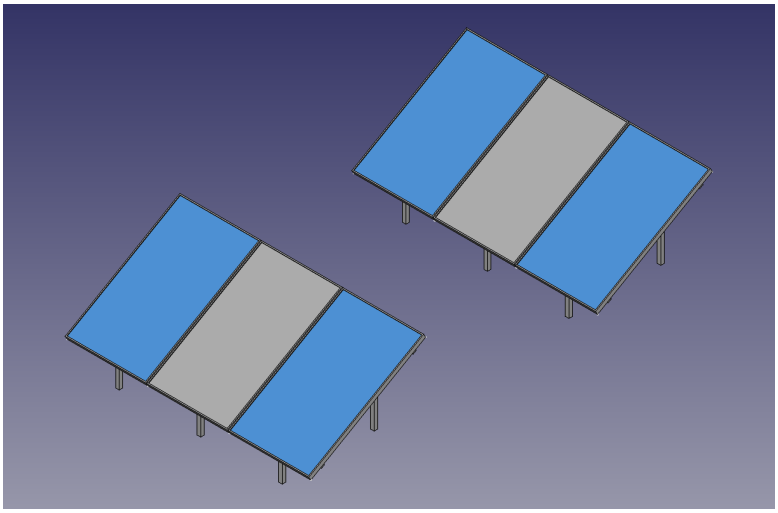

Figure 4.5: Two rows of arrays (3 by 2).

Two geometries were analyzed: the one shown in the figure above and a more complex one that

has two rows of 9 panels each, which means that there are five replicas of the reference array plus the reference array. This geometry, displayed in figure 4.6, simulates a much more similar case to what can be observed in solar plants. For this reason, calculations regarding PV modules temperature prediction and output power variation were only developed for the later-mentioned geometry.

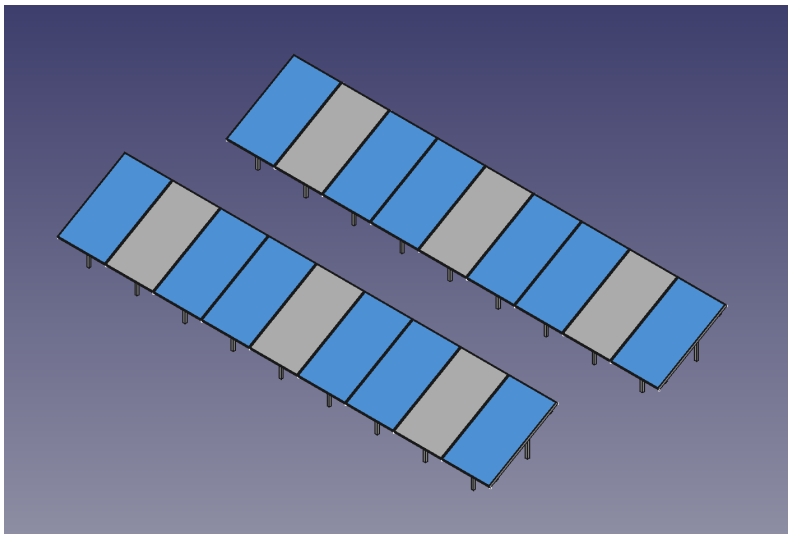

Figure 4.6: Two rows of arrays (9 by 2).

For the purpose of studying wind flow around the panels, CFD simulations demand that the geometry created has to be inside a wind tunnel. This thematic is approach in the section that follows.

4.2 Wind Tunnels

A wind tunnel is a structure (rectangular, circular or elliptical) with air moving inside and it is used to copy the actions of an object that is stationary or moving, having air flowing around it. Most of the times, air movement is produced by powerful fans or by compressed air; the object is always fastened to the tunnel so that it will stay in place [66]. Wind tunnel experiments are based on the principle of relativity enunciated by Isaac Newton, in 1687: ”the forces exerted on a solid immersed in a fluid and the fluid are the same either the solid moves with a certain speed through the fluid at rest, or the fluid moves, with the same relative velocity to the solid that it is immobile” [67, p. 1].

Nowadays, physical wind tunnels experiments are often used in parallel with CFD techniques in order to improve the reliability of results, due to the fact that both methods can be used to validate each other.

Several parameters should be respected when sizing a wind tunnel and these conditions become fundamental when simulating flows inside a wind tunnel through CFD methods. This being said, migrating the CAD geometry to Fusion 360 allowed a simpler creation of the tunnel structure. Autodesk, the company that created this software, proposes the following (assuming h as the total height of the CAD

model, w its total width and l its total length) [68]:

1. $3h <$ Tunnel height $< 4h$ – model sitting on the floor (z = 0);
2. $5w <$ Tunnel width $< 7w$ – model in the center;
3. Tunnel length from the front (inlet) to the object = $2l$ (in the direction of flow);
4. Tunnel length from the object to the back (outlet) = $4l$ (in the direction of flow).

These dimensions allow a correct flow around the object. When the tunnel is not sized properly, its walls may artificially accelerate the flow around the model and prevent the formation and shedding of vortices downstream of the model, thus representing a non-viable situation.

Having all these factors in mind, two wind tunnels (one for each geometry) were created – in figure 4.7 and 4.8.

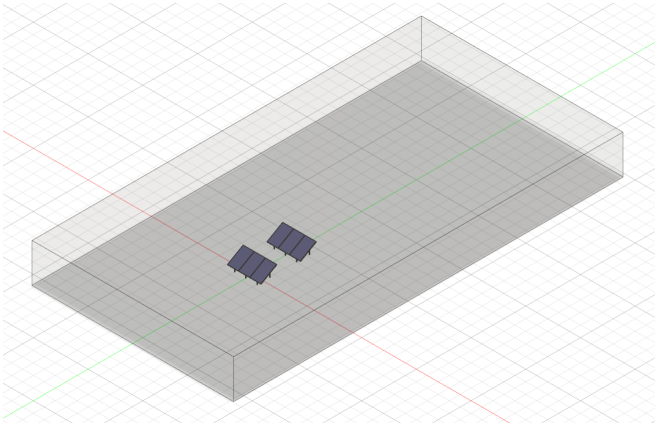

Figure 4.7: Wind tunnel for 3 by 2 geometry.

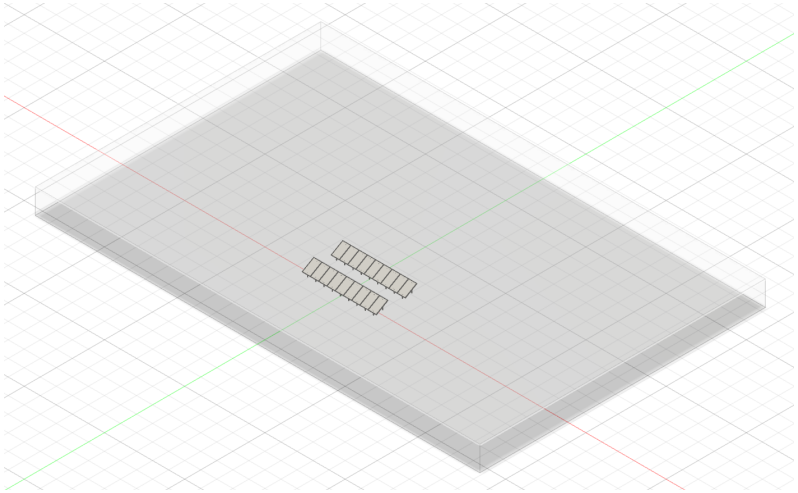

Figure 4.8: Wind tunnel for 9 by 2 geometry.

As it can be observed, the second geometry has a much wider tunnel, once the width of the 9 by 2 design is approximately thrice the width of the 3 by 2. Owing to the fact that the length of the PV geometries is the same (side-view: first row, spacing and second row), wind tunnels length is necessarily the same. Concerning the height, an equivalent situation happens: as the height of the two designs is the same, wind tunnels height are equal.

Before running simulations, the geometries created have to go trough a process called meshing, which plays a significant role when it comes to the final results. For this task, the CAD geometry was exported from Fusion 360 and imported to Autodesk CFD. All the relevant details concerning this procedure are explained below.

4.3 Meshing

Meshing is the process of dividing a CAD model into small cells that can be used to discretize a domain in order to simplify a geometry's complexity. The objective is to get a 3D geometry equivalent to the one projected in the first place, but divided into multiple elements. When ensuring the accuracy of simulations, mesh quality is critical – the more detailed the mesh is, the more realistic the shape formed by the numerous cells is, which implies higher fidelity results [69].

Mesh generation allows solving simulations due to the fact that the geometry is divided into mathematically defined shapes. As softwares aren't ready to solve the problem for the entire CAD model at once, the governing equations are applied to each of these volumes that are previously predicted either by the software itself (automatically) or with some help from the user. Given that Autodesk CFD has a very good built-in mesh generation tool, the mesh for each of the models only needed to be refined so as to provide reliable results. 3 layers of refinement with a layer factor of 0.45 and an automatic layer gradation were imposed. The local mesh refinements (blue points) can be verified in figure 4.9 and 4.10.

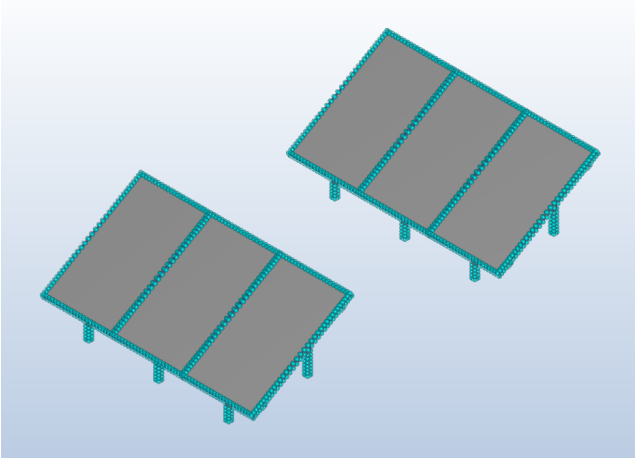

Figure 4.9: Refinement of the 3 by 2 geometry.

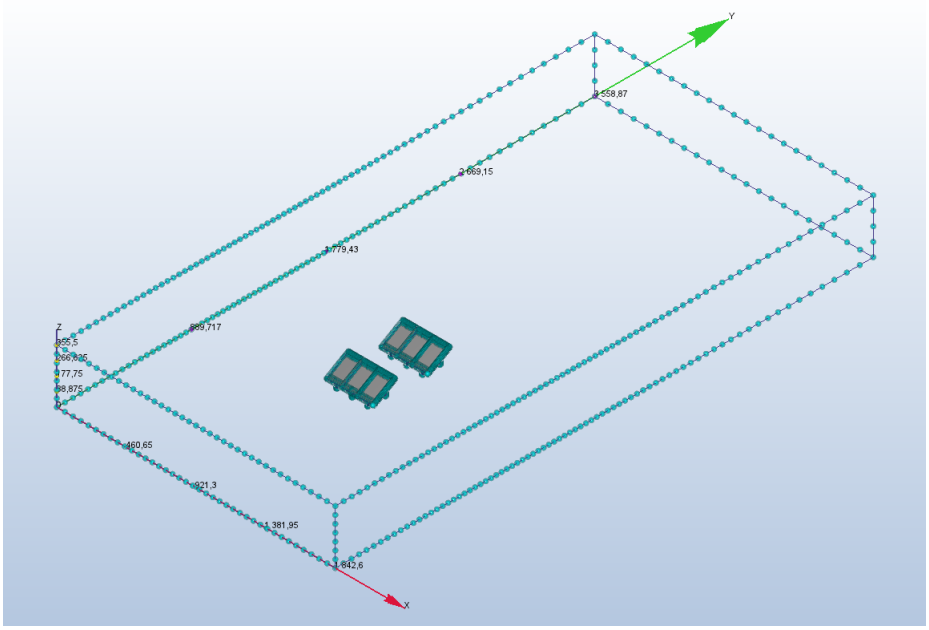

Figure 4.10: Refinement along the wind tunnel edges for the 3 by 2 geometry.

Figure 4.9 shows a local refinement applied directly to the geometry. In figure 4.10 it can be observed that there is a higher density of the meshing grid points (applied to the wind tunnel) for the surrounding area of the geometry. This technique was applied to both of the geometries (3 by 2 and 9 by 2), but there is no need for showing both cases as the procedure is equivalent.

Apart from the referred refinements, it was achieved a good quality mesh out-of-the-box. The mesh of each model can be observed in figure 4.11 and 4.12.

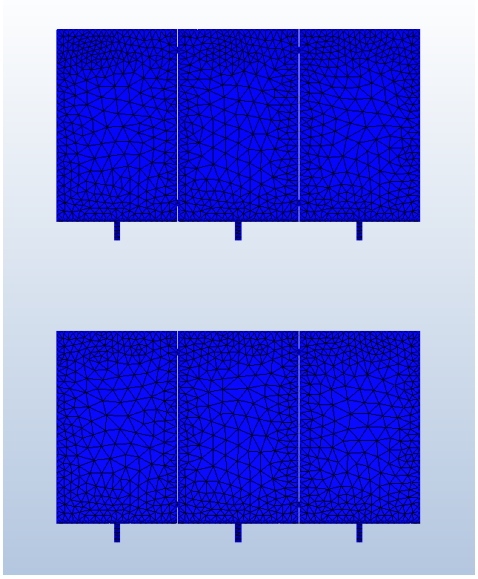

Figure 4.11: 3 by 2 geometry after mesh generation.

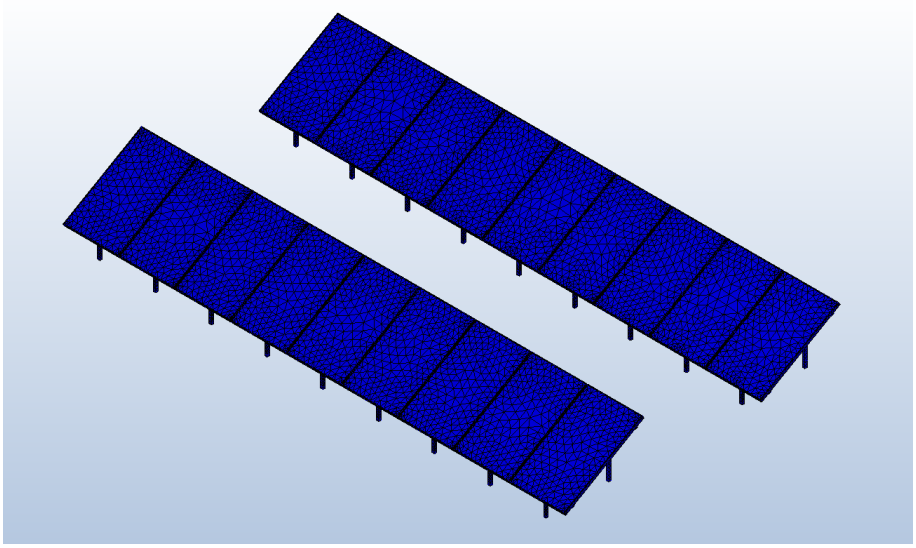

Figure 4.12: 9 by 2 geometry after mesh generation.

It can be seen that the 3D geometries produced by mesh generation embody the CAD geometries created just as they are, despite of their multiple elements. For the smaller one, 299051 total elements were generated; for the other one, 607469.

Another important task of the pre-processing stage is the solver setup. This is the point were the conditions of the problem to be solved are defined, as covered in the following section.

4.4 Solver Setup

Solver setup is a fundamental step of a CFD analysis because fluid material properties, boundaries and the flow physics model are defined in order to run simulations.

The first part is to dictate fluid material properties. As a thermal analysis will not be performed, the materials assigned to the rows of PV panels are negligible – the geometry is only defined as a solid. However, the fluid inside the wind tunnel must be air, obviously – when attributing this material, the properties inside of the tunnel are instantly recomputed by the software. Wind tunnel structure does not present any requirement in what concerns materials; but in spite of that, it inevitably needs boundaries designation, which is a process based on imputing physical conditions to the boundaries of the flow domain – the so-called boundary conditions.

Boundary conditions are mandatory constraints for the solution of a boundary value problem, i.e., a domain whose boundaries are known and where a system of differential equations (or just one differential equation) is to be solved. This type of problem is usually opposed to the ”initial value problem”, that is commonly associated with problems to be solved in time, whereas the boundary value problem

refers to a solution in space [70]. Boundaries determination is intrinsically connected to the flow physics model, which is detailed right away.

With the understanding that wind is a fluid flow, when simulation the wind influence on photovoltaic panels, it was decided to neglect its laminar phase, since it is well known that the laminar phase of a flow (smooth path with no disruption between adjacent paths) is much smaller than its turbulent one (chaotic path that comprises eddies, swirls and flow instabilities) in the type of problem studied here; most engineering flows are turbulent [71]. The distinction between types of fluid flows was studied by Osborne Reynolds, in the nineteenth century, when he discovered the number that predicts fluid flow based on the static and dynamic properties present in equation (4.2):

$$Re = \frac{\rho \cdot V \cdot D}{\eta} \tag{4.2}$$

Being Re the Reynolds number, ρ is the fluid density in kg/m^3, V is the fluid velocity in m/s, D is the pipe diameter in m and η is the fluid dynamic viscosity in kg/(m·s). For Reynolds numbers smaller or equal to 2300, the flow is considered laminar, between 2300 and 4000, exclusive, it is considered a transient regime and for numbers higher or equal to 4000, the flow is considered turbulent [72].

For the type of simulation under study, it is widely known that the Reynolds number is in the turbulent flow range. Thereby, a turbulent flow k-epsilon (which is the default turbulence model in Autodesk CFD) was applied as an external flow in the longitudinal direction of the wind tunnel. The standard $k-\epsilon$ model was chosen by virtue of its characteristics: it gives accurate predictions on distribution of speed around CAD geometries [73] and it is a general purpose model (the most used) that performs well for a large number of applications. The $k-\epsilon$ model is part of the Reynolds-Average Navier Stokes (RANS) family of turbulence models and both letters that name it (k and ϵ) refer to two transport equations that are solved upon its usage: turbulent kinetic energy – energy in turbulence – and turbulent dissipation rate – rate of dissipation of turbulent kinetic energy, respectively. The turbulent kinetic energy is given by equation (4.3) [72]:

$$k = \frac{3}{2}(V \cdot I)^2 \tag{4.3}$$

Where V is the fluid velocity and I is the turbulence intensity, which can be defined by equation (4.4):

$$I = \frac{v'}{V} \tag{4.4}$$

v' is the root mean square of the turbulent velocity fluctuations, expressed by equation (4.5) and V is calculated by equation (4.6), where the index of each variable represents its component along the referred axis [74]:

$$v' = \sqrt{\frac{1}{3}\left({v'_x}^2 + {v'_y}^2 + {v'_z}^2\right)} = \sqrt{\frac{2}{3}k} \tag{4.5}$$

$$V = \sqrt{V_x'^2 + V_y'^2 + V_z'^2} \tag{4.6}$$

The turbulent dissipation rate, ϵ, can be written as equation (4.7) shows:

$$\epsilon = C_\mu{}^{\frac{3}{4}} \cdot \frac{k^{\frac{3}{4}}}{l} \tag{4.7}$$

In which C_μ is a model intrinsic constant usually equal to 0.09 (value used in simulations) and l is the turbulent length scale – it defines the size of large energy-containing eddies in the flow. The turbulent viscosity, v_t is calculated by equation (4.8):

$$v_t = 0.09\frac{k^2}{\epsilon} \tag{4.8}$$

When assigning the turbulent flow model to the tunnel, the user must specify the boundary conditions for wind tunnel walls, as mentioned before. In order to get the results intended, the following conditions were applied, having in mind that they are related to the $k - \epsilon$ model:

1. inlet – velocity type, with magnitudes of W_{max} and W_{avg}, as specified in Wind (steady-state);
2. outlet – pressure type, equal to zero (steady-state);
3. top and sides – slip/symmetry type.

Once the front of the PV geometry is facing the inlet, wind flow is parallel to planes xOy and yOz and perpendicular to xOz, flowing from the inlet to the outlet. Note: these axis can be observed in figure 4.10.

In this chapter, the steps that define the first (and more complex/time consuming) stage of a computational fluid dynamics analysis were explained and detailed as it seemed relevant and appropriate. Its four main topics, here documented as sections (CAD modeling of the PV geometry, sizing of wind tunnels, geometry mesh generation and solver setup) manifest their importance when running simulations, being reflected in the final results. Having all of these concepts been clarified, the next stages – processing and post-processing – are detailed in the following chapter, Experimental Results.

5

Experimental Results

Contents

Experimental results are the product of simulations and simulations themselves, which were prepared in the previous chapters. These results are presented by order of completion, being organized into three sections: wind flow around the CAD geometries, the predicted modules temperature according to the different module temperature prediction models and the output power variation taking into account datasheets parameters and the values of temperature calculated.

5.1 Wind Flow

Wind flow around the PV arrays was analyzed for each geometry, taking into consideration the two aforementioned wind velocities at the inlet: W_{avg} = 4.06 m/s and W_{max} = 17.55 m/s. After several hours of running time, the simulations regarding both geometries were ready to some post-processing. This being said, in order to extract valuable information about turbulent flow behavior, a vertical plane – parallel to yOz and perpendicular to xOz – was applied to the wind tunnel, for each geometry and for each inlet wind speed. This generates a cross section inside the tunnel's volume, where it can be observed the wind flow pattern. With the purpose of obtaining a general wind flow distribution around the whole geometries, a rectangular grid of points was defined at the inlet. Each of these points generates a path across the tunnel for the corresponding wind element point, creating a continuous line. These different cases are displayed next; they are organized by geometry so that content organization favors the comprehension of comparisons between them. Since the 9 by 2 geometry will be further studied, the analysis begins with the simpler design, which depicts a simulation of a real case and gives fundamental insights about what to expect in more complex photovoltaic arrangements.

5.1.1 3 by 2 Geometry

In what the first CAD model is concerned, its simulations results for W_{avg} are shown in figure 5.1 and figure 5.2. For the first one, the vertical plane is aligned with the central module of both rows, given that they are parallel (x and z coordinates are equal). For the later one, the plane is aligned with the tip module of each array. The left side scale indicates the velocity magnitude in cm/s, starting in 0 cm/s and ending in 514.366 cm/s for all the figures that refer to this wind speed value.

It can be observed that the wind shadow phenomenon introduced in Related Studies occurs, which implies a decrease in wind speed right after the first array, thus leading to a lower wind intensity for the second row. When inspecting the wind behavior close to the front PV module, it is possible to verify that wind has higher speed magnitudes in the upper portion of its face. Although this also happens to the equivalent panel of the second row, the magnitudes are much different, which will cause disparities between temperatures of the modules, because wind speed is known to have an influence in this factor, as it was introduced earlier and as it will be demonstrated in Module Temperature Prediction.

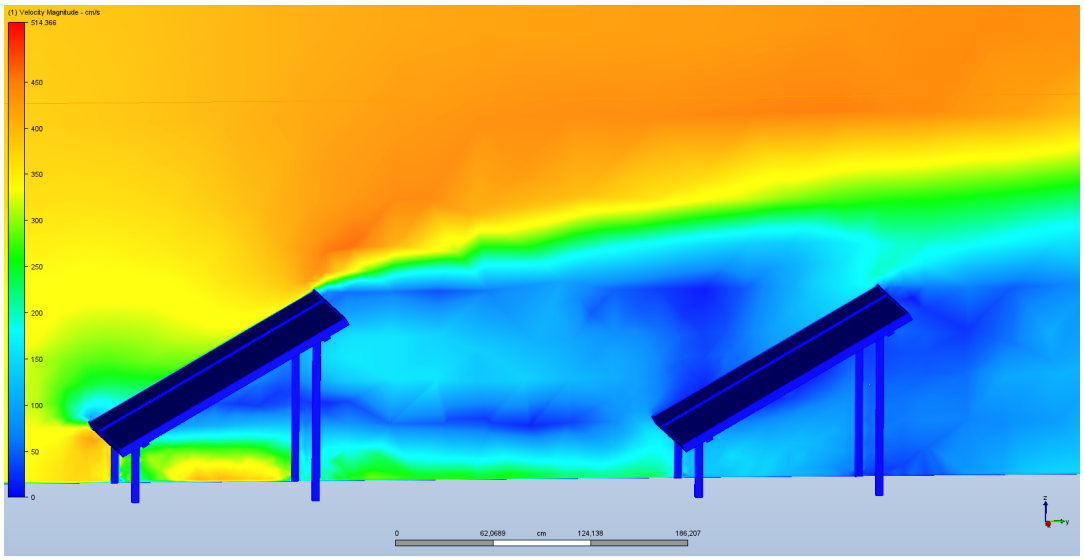

Figure 5.1: Wind flow for a vertical panel aligned with central module of the 3 by 2 geometry – W_{avg}.

It can be said that despite the fact that turbulent flows are not likely to be perfectly predictable, there is approximately a symmetry of wind flow distribution thus wind speed distribution from the middle of each row to each of its extremities. Consequently, there is no need to show wind flow simulations for both of them.

By examination of the cross section that represents wind flow for the surroundings of the tip modules of each row, it can be verified that the wind shadow effect is attenuated, hence the rear panel presents higher speed values near its face if compared to the central module. At the same time, it is clear that wind has a not so different behavior for all the front row modules when compared to the rear set.

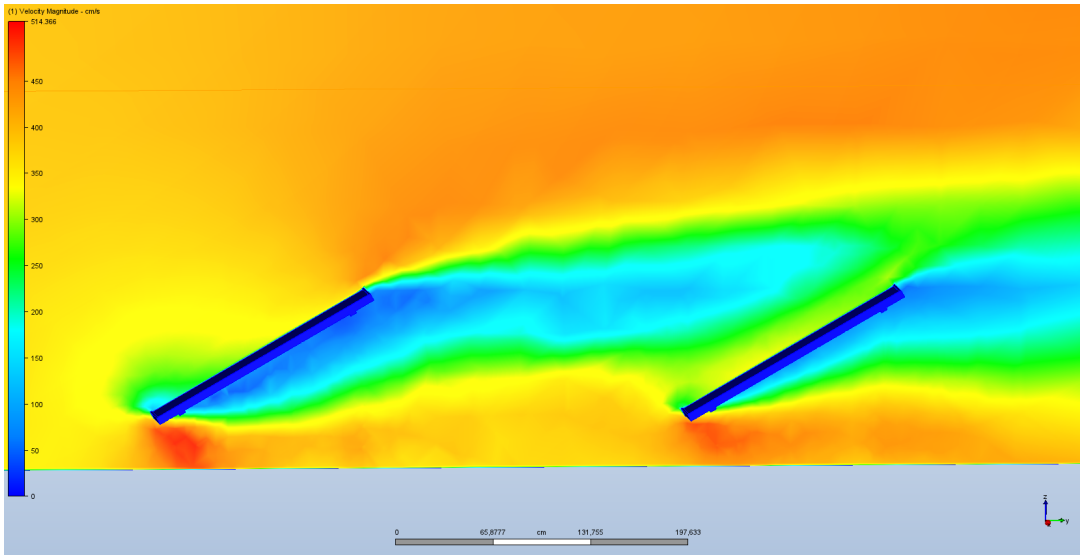

Figure 5.2: Wind flow for a vertical plane aligned with tip module of the 3 by 2 geometry – W_{avg}.

Figure 5.3 shows the wind flow around the geometry by a three dimensional perspective, allowing the perception of wind movement along the wind tunnel when crossing the whole PV structure. It confirms that there is wind shadowing between rows of panels, by two factors: reduction of lines density and mitigation of wind speed.

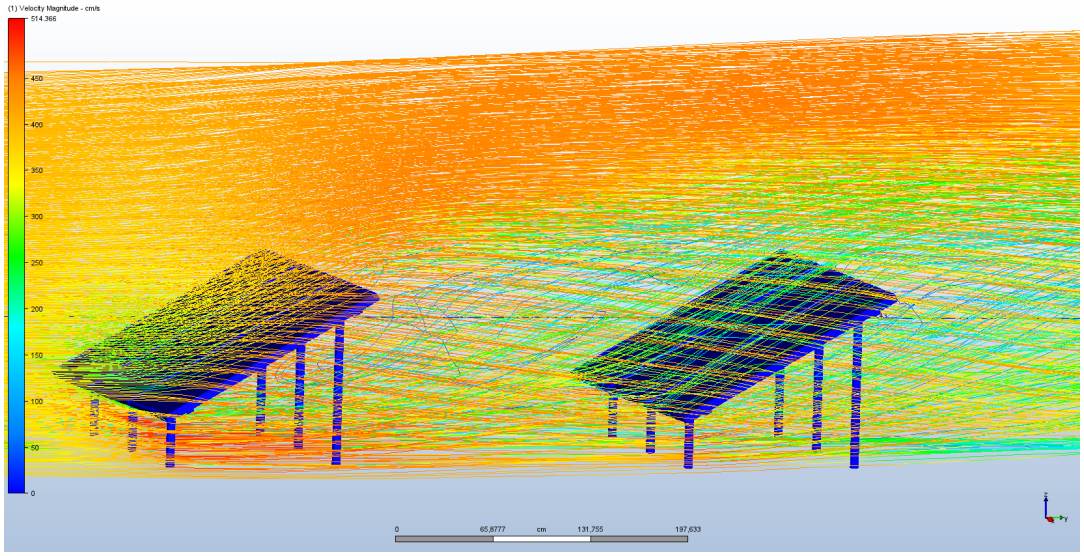

Figure 5.3: Wind flow for the 3 by 2 geometry – W_{avg}.

Figure 5.4, which is a side view of the previous one, makes evident the appearance of swirls that differ from the common motion of the fluid, as they are represented mostly by blue lines after each array. These swirls are the so-called eddies in fluid mechanics. Their energy is successively transferred from large eddies to smaller ones until it is dissipated [75].

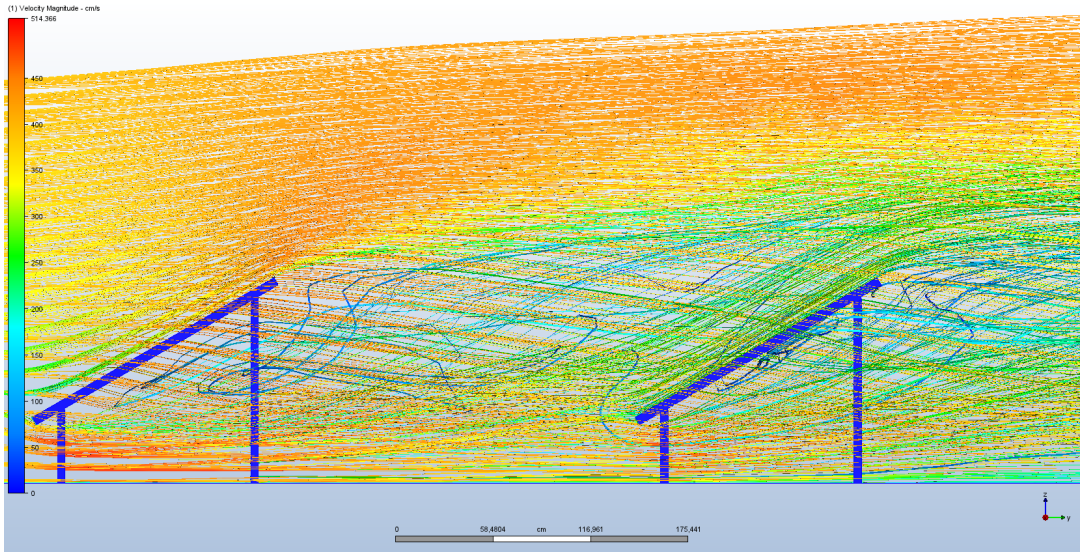

Figure 5.4: Side view of wind flow for the 3 by 2 geometry – W_{avg}.

In order to collect the exact values of wind speed for each module, a parallel plane to the surface of the panels was applied. With this, Autodesk CFD allows the selection of an area (user-defined) whose average wind speed value can be calculated by the software. Taking this tool into consideration, figures 5.5 and 5.6 show the plane right above the modules surfaces for the front and rear row, respectively.

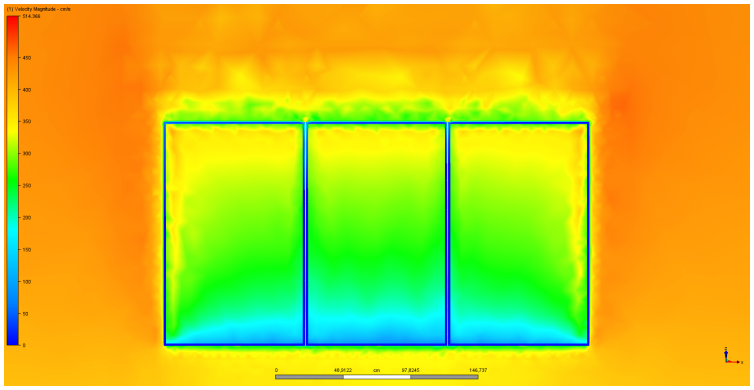

Figure 5.5: Wind speed for first row of panels – W_{avg}.

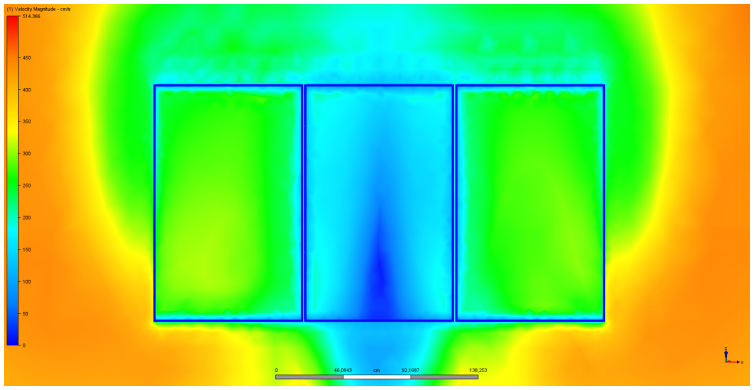

Figure 5.6: Wind speed for second row of panels – W_{avg}.

Considering that the numbering of panels is done from left to right and that it starts in the left tip panel of the first row, the exact wind speeds extracted from the software are displayed in table 5.1. The parcel *Ratio* indicates the ratio between the wind speed that is calculated and the inlet speed value.

Table 5.1: Wind speed for each panel – W_{avg}.

	Wind speed (m/s)	**Ratio**
Panel 1	2.77001	0.6823
Panel 2	2.57374	0.6339
Panel 3	2.76165	0.6802
Panel 4	2.69321	0.6634
Panel 5	1.34411	0.3311
Panel 6	2.68057	0.6602

Regarding the simulations for the 3 by 2 geometry with the second value of wind speed (W_{max}), figure 5.7 and figure 5.8 show similar representations of wind flow around the solar panels and their support structure in comparison with the last case, as it was expected. Nevertheless, velocity magnitudes are obviously distinct. This being said, its legend indicates a scale of velocity magnitude that goes from 0 cm/s to 2243.04 cm/s.

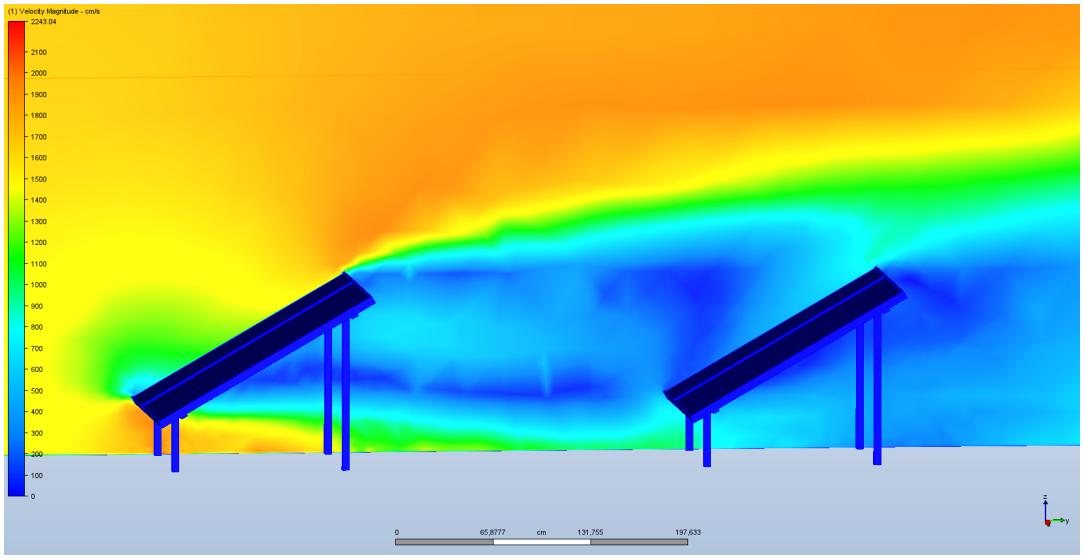

Figure 5.7: Wind flow for a vertical panel aligned with central module of the 3 by 2 geometry – W_{max}.

Identically to what can be recognized in figures 5.1 and 5.2, wind speeds for the surroundings of the rear modules present much lower values than the ones that are verified for the front row. It is also noticeable that wind shadow effect is reduced when closer to the tips of the arrays.

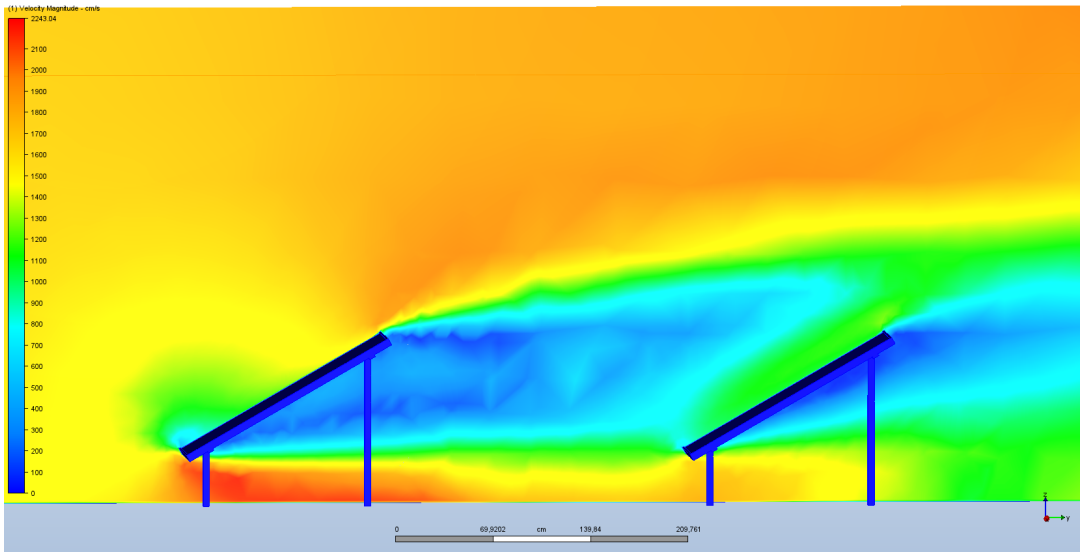

Figure 5.8: Wind flow for a vertical panel aligned with central module of the 3 by 2 geometry – W_{max}.

As it was done for the lower inlet wind speed, it is also shown the general wind flow for the maximum average speed, figure 5.9.

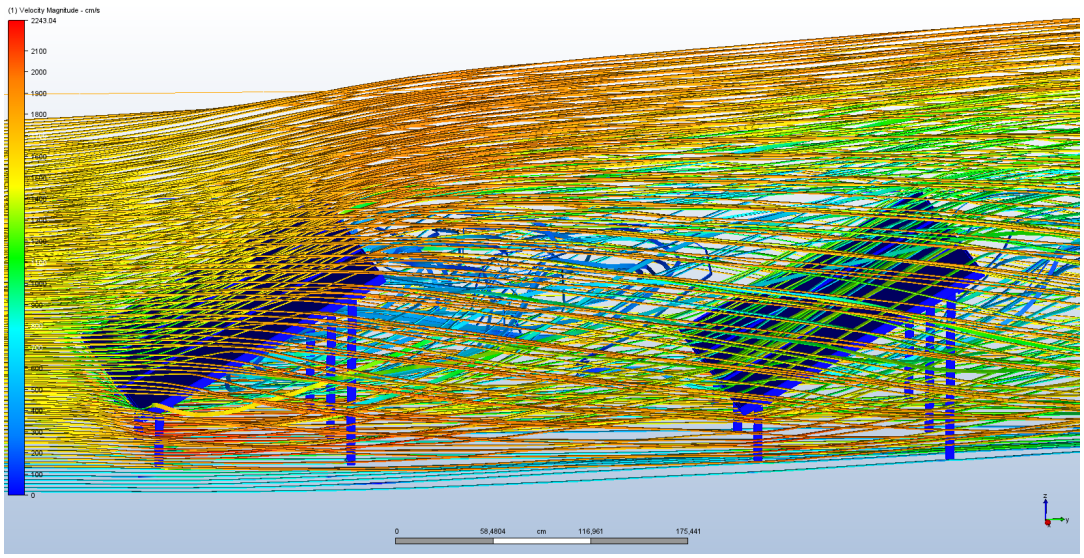

Figure 5.9: Wind flow for the 3 by 2 geometry – $W_{\max}$.

It can be noticed that the wind flow is similar to the previous case, but it has a lot more eddies due to a much higher intensity of turbulent phenomenons, since the wind speed value at the inlet is approximately 4.3 times the average average wind speed.

The process executed with the aim of collecting the average wind speed value for each of the modules surfaces vicinity was repeated. Given that the distribution of wind speed along the surfaces of the panels is really similar to the one shown in figures 5.5 and 5.6 (for the lower wind velocity), the corresponding illustrations are omitted. Having said that, the software generated the values exhibited in table 5.2.

Table 5.2: Wind speed for each panel – $W_{\max}$.

	Wind speed (m/s)	**Ratio**
Panel 1	12.3322	0.7027
Panel 2	11.4047	0.6498
Panel 3	12.2184	0.6962
Panel 4	12.1172	0.6904
Panel 5	5.9081	0.3366
Panel 6	12.0584	0.6871

By comparison of the two last tables, their similarity in what the ratio is concerned is truly evident. There is a significant decrease of wind speed for the central module of the second row (panel 5) but the effective difference between panel 1 and 4 and between 3 and 6 is almost unnoticeable; although the distribution of wind speed may not be so alike (figure 5.5 and 5.6), the average wind speed values are.

5.1.2 9 by 2 Geometry

The 3 by 2 geometry presents a reduced complexity when compared to the geometry covered in this subsection. Although it can represent a real-life situation in such a manner that the simulations results detailed before are a very coherent starting point for what can be expected for other arrangements, the most common designs found in solar plants are clearly more similar to this second one. This being said, each of the tasks performed for the simpler CAD model were replicated to the 9 by 2 geometry. Herewith, even though wind flow behavior shows identical characteristics for both of the cases, relevant differences will be pointed out.

Starting by the analysis of simulations related to W_{avg}, a vertical plane was applied to the wind tunnel, as it can be seen in figure 5.10, generating a cross section along the PV structure and the tunnel.

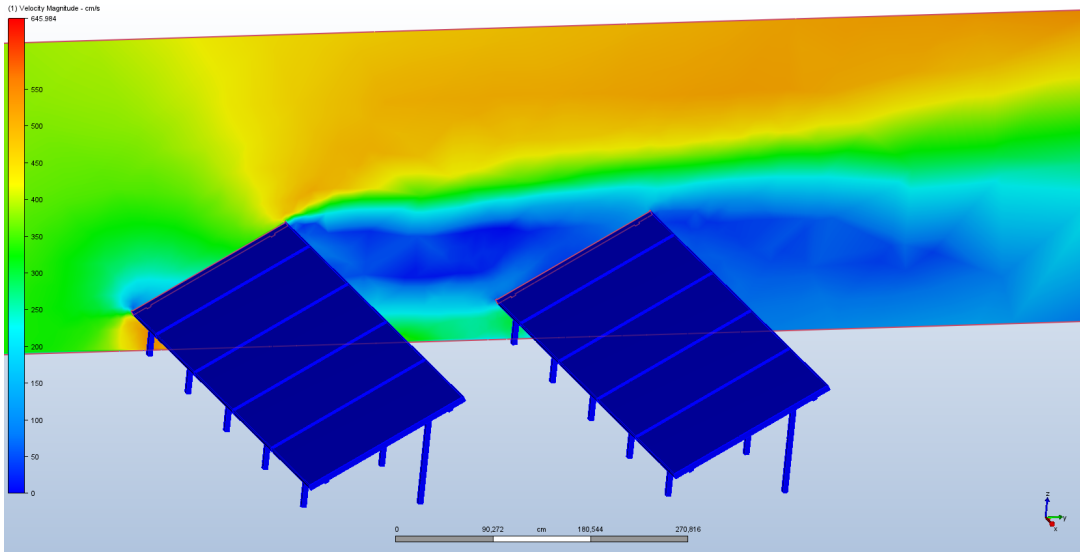

Figure 5.10: Wind flow for a vertical panel aligned with central module of the 9 by 2 geometry – W_{avg}.

This figure depicts the wind flow for the area represented by the plane. The scale displayed in the left side of the figures that illustrate the average average wind speed at the inlet indicates the velocity magnitude, starting in 0 cm/s and goes up to 645.984 cm/s. As it was done for the previous geometry, the plane is aligned with the central module of the 9 by 2 geometry. Once again, the wind shadow effect can be observed due to the much lower wind speed verified for the surroundings of the rear module.

As mentioned before, there is an approximate symmetry in wind flow distribution from the central module to the ones in the extremities – this occurs for both rows. Figure 5.11 shows wind flow when the vertical plane is aligned with the tip modules. By its inspection, it is possible to see that just like with the preceding geometry, the wind shadowing effect is almost null.

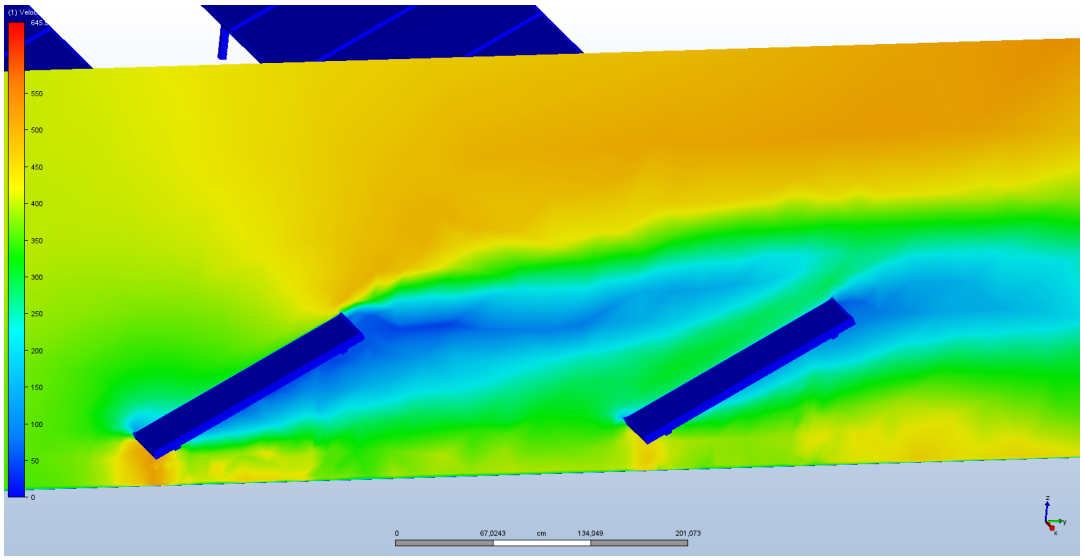

Figure 5.11: Wind flow for a vertical panel aligned with tip module of the 9 by 2 geometry – W_{avg}.

In order to have a wide perspective of the wind flow around the whole CAD structure, the procedure of creating a rectangular grid of points in the inlet was repeated, but now for a much larger width. The result obtained is represented in figure 5.12, in which the aforementioned eddies that are characteristic of this type of wind profile model can be observed, just like the decrease in density of lines between both rows, indicating a lower intensity of wind loads.

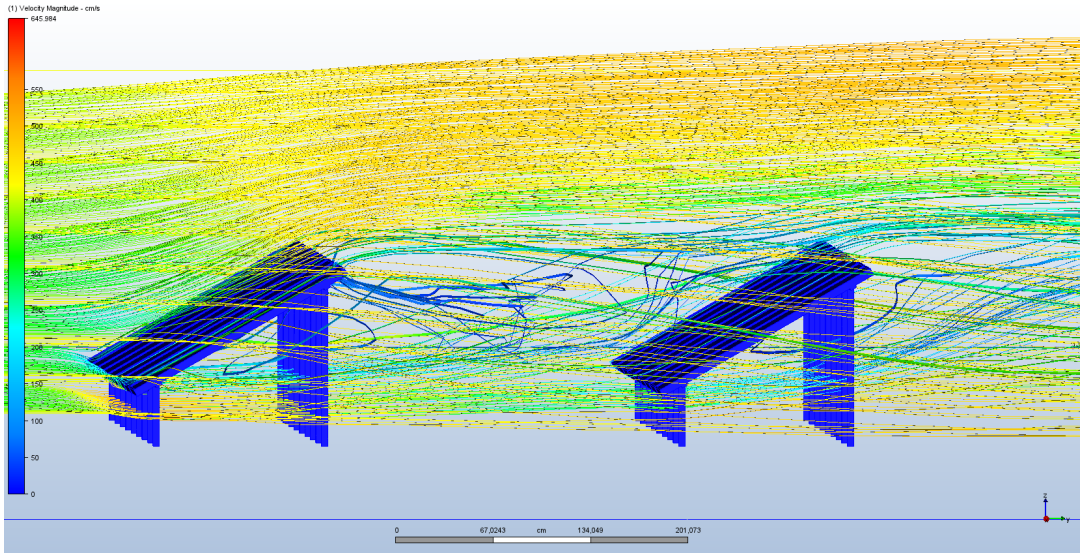

Figure 5.12: Wind flow for the 9 by 2 geometry – W_{avg}.

With the purpose of collecting the wind speed values for each panel of the geometry, the parallel plane to the surface of the modules was applied anew, granting the calculation of the average wind speed for the vicinity of each panel by the software. Figures 5.13 and 5.14 demonstrate the planes that

were used in this labor.

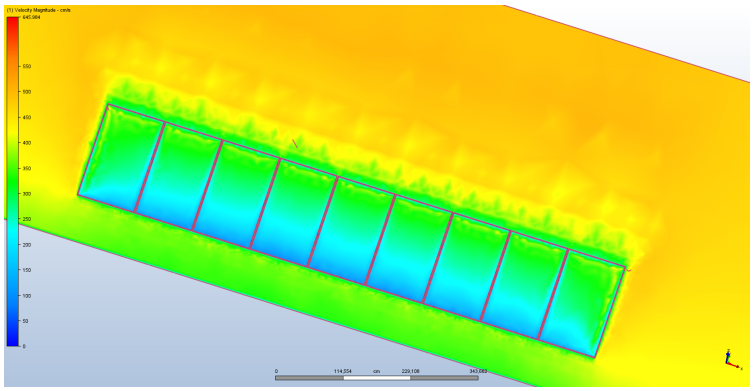

Figure 5.13: Wind speed for first row of panels – W_{avg}.

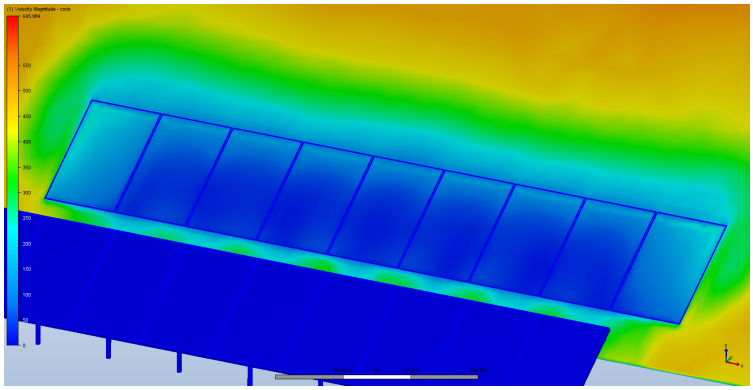

Figure 5.14: Wind speed for second row of panels – W_{avg}.

Remembering that the parcel *Ratio* corresponds to the ratio between the wind speed value exported from Autodesk CFD and the wind velocity at the inlet, the concrete values of wind speed calculated by the software, for each module, are presented in table 5.3.

Table 5.3: Wind speed for each panel – W_{avg}.

	Wind speed (m/s)	**Ratio**		**Wind speed (m/s)**	**Ratio**
Panel 1	2.8307	0.6972	Panel 10	2.0932	0.5156
Panel 2	2.5662	0.6321	Panel 11	0.8621	0.2123
Panel 3	2.4935	0.6142	Panel 12	0.7557	0.1861
Panel 4	2.4389	0.6007	Panel 13	0.7445	0.1834
Panel 5	2.4498	0.6034	Panel 14	0.7180	0.1769
Panel 6	2.4767	0.6100	Panel 15	0.7561	0.1862
Panel 7	2.5241	0.6217	Panel 16	0.7959	0.1960
Panel 8	2.5407	0.6258	Panel 17	0.8583	0.2114
Panel 9	2.7356	0.6738	Panel 18	2.1541	0.5306

Analogously to what was noticed for the previous geometry, an abrupt difference between the wind speeds registered for the tip modules of the rear row (panels 18 and 10) and the remaining can be verified. There is a clear difference between this scenario and the one studied in the previous subsection: the ratios observed for the tip panels of each row (1 and 10, 9 and 18) decrease substantially from the front to the rear row – a situation that did not happen for the smaller geometry.

Having all the pertinent results showcased for W_{avg}, the last simulations in what the maximum average wind speed at the inlet (W_{max}) is concerned are shown next. The velocity magnitude scale displayed in the left side of the following figures starts in 0 cm/s and has a maximum value of 2921.97 cm/s. For the last time, a vertical plane was applied to the wind tunnel, creating a cross section along the structures volumes. Figure 5.15 depicts the plane aligned with the central panels of the photovoltaic arrangement and figure 5.16 when it is aligned with the tip panels of each row.

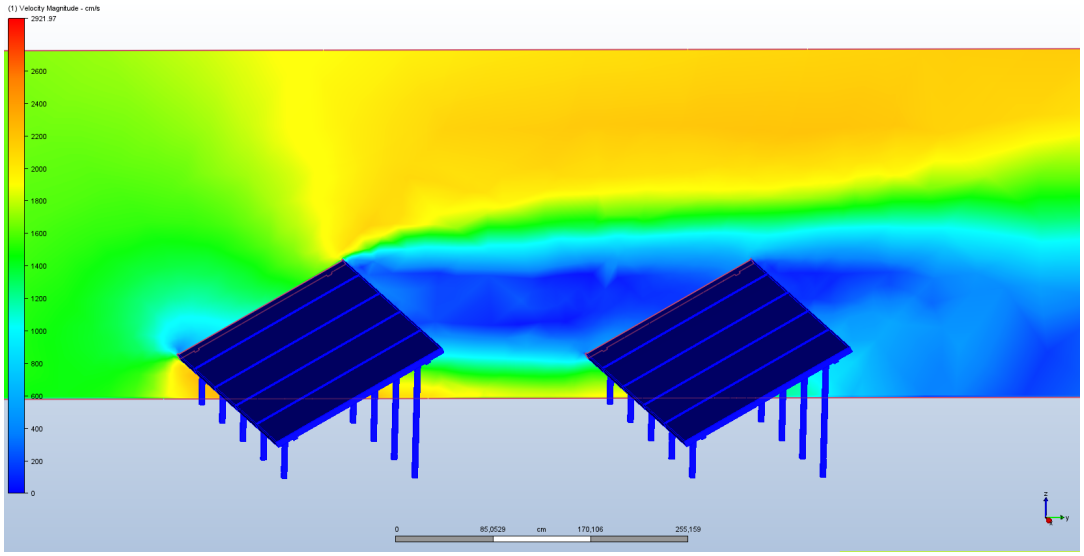

Figure 5.15: Wind flow for a vertical panel aligned with central module of the 9 by 2 geometry – W_{max}.

In this first figure, higher values of wind velocity can be seen close to the front row modules when compared to the rear row, as it was predictable. Just like it happened with the situations analyzed before, the upper sections of the PV panels surfaces vicinity display higher wind speeds, colored by green areas, as their lower sections have a more bluish tonality, which express lower magnitudes. For the rear row, blue areas are a constant because of wind shadowing. Figure 5.16 shows that the tendency of this phenomenon to be attenuated when closer to the extremities panels is pretty transparent.

In order to see the differences between the general wind flow across the totality of the solar photovoltaic model for each wind speed, a rectangular grid at the inlet of the tunnel was created, one more time. Hereupon, figure 5.17 illustrates a three-dimensional perspective of the wind flow inside the tunnel.

In comparison with figure 5.12, the propensity of eddies generation for higher wind speed magnitudes

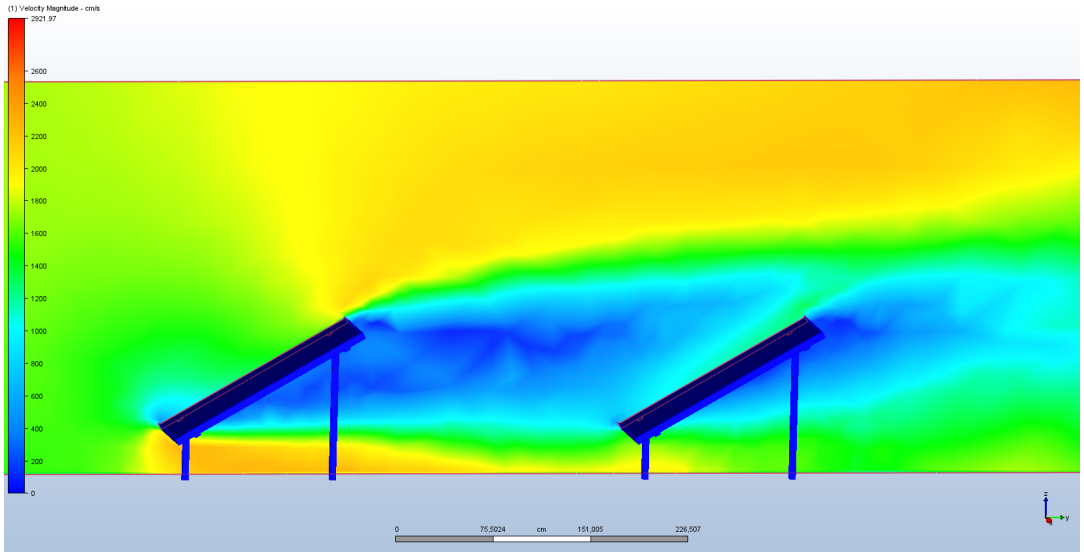

Figure 5.16: Wind flow for a vertical panel aligned with tip module of the 9 by 2 geometry – W_{max}.

becomes unmistakable. As mentioned precedently, these swirls become stronger due to the presence of high intensity turbulent circumstances. There is a lower density of lines after each panel, which reflects the obstruction of flow motion, produced by the photovoltaic structures.

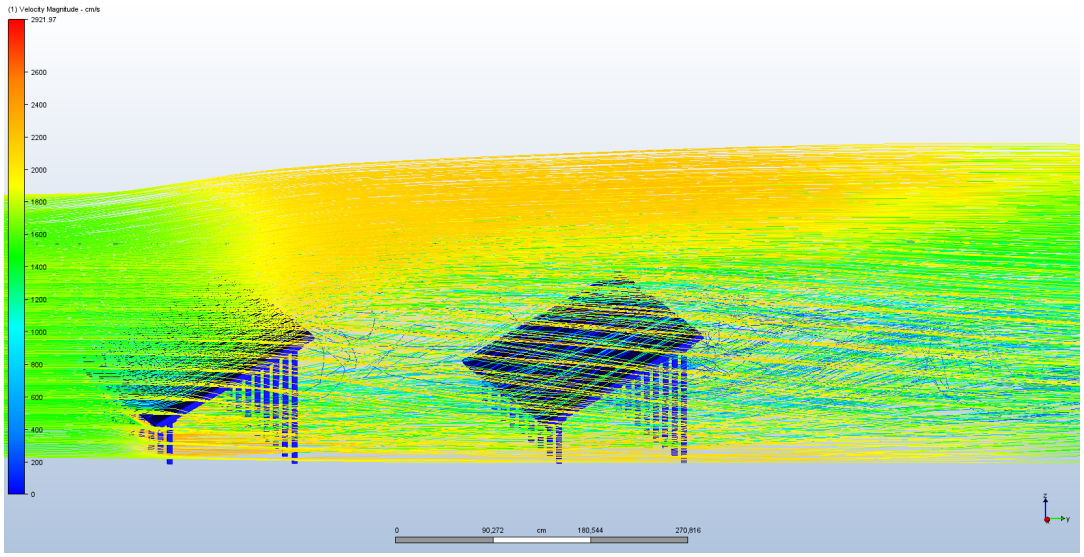

Figure 5.17: Wind flow for the 9 by 2 geometry – W_{max}.

The last step of data collecting pertains to the acquisition of wind speed values for all the panels surfaces vicinity. A parallel plane to the modules surface was applied to each row. Figures 5.18 and 5.19 display these panels and the consequent wind speed distribution for each set of coordinates – front row and rear row, respectively.

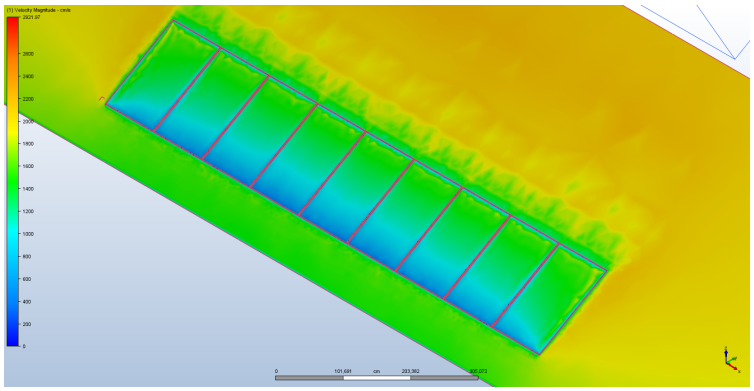

Figure 5.18: Wind speed for first row of panels – W_{max}.

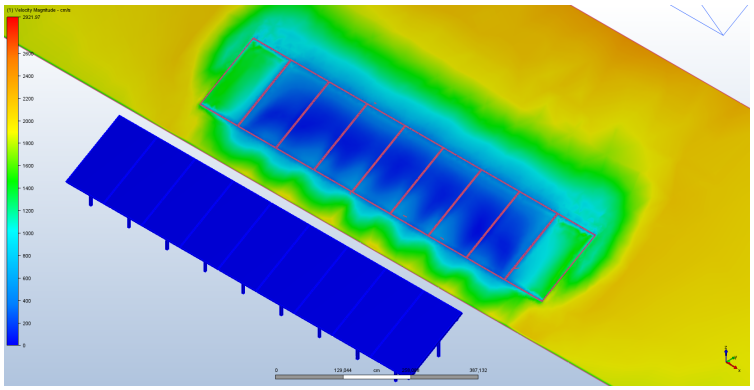

Figure 5.19: Wind speed for second row of panels – W_{max}.

All the average wind speed values calculated by Autodesk CFD according to the figures shown above are displayed in table 5.4. In contrast with table 5.3, for a higher wind velocity at the inlet, the wind shadow effect is reduced for the tip panels, which leads to a similar ratio when comparing wind speed for panel 1 with 10 and panel 9 with 18 – relations that are closer to what was verified for the first geometry.

Table 5.4: Wind speed for each panel – W_{max}.

	Wind speed (m/s)	**Ratio**		**Wind speed (m/s)**	**Ratio**
Panel 1	13.2141	0.7529	Panel 10	12.3679	0.7047
Panel 2	11.965	0.6818	Panel 11	3.4115	0.1944
Panel 3	11.5708	0.6593	Panel 12	2.6822	0.1528
Panel 4	11.4064	0.6499	Panel 13	2.8797	0.1641
Panel 5	11.4009	0.6496	Panel 14	2.8360	0.1616
Panel 6	11.4496	0.6524	Panel 15	2.9946	0.1706
Panel 7	11.6691	0.6691	Panel 16	2.8800	0.1641
Panel 8	11.9045	0.6783	Panel 17	3.2980	0.1879
Panel 9	13.0969	0.7463	Panel 18	12.2337	0.6971

This finishes the process of collecting data to be used in calculations related to the modules temperature prediction. These calculations are covered in the following section.

5.2 Module Temperature Prediction

Regarding the prediction of panels temperature, the prediction models introduced in Related Studies and summarized in chapter 3 are the main ingredient of calculations, given that their characteristics are what allows the comparison between different temperatures for the various wind speeds that were collected in the previous section.

This being said, the temperature predictions were only performed for the second geometry (9 by 2), which depicts a more common case in solar plants. In addition to that, due to the similarities verified for wind flow for both of the geometries under study, it would be almost redundant to calculate the temperatures for each geometry. That being so, the calculations for the 9 by 2 geometry were done according to the following:

- Module temperature forecast according to each prediction model;
- For each prediction model, each PV technology was studied;
- For each PV technology, calculations were done for W_{avg} and W_{max}.

Which gives a total of 864 calculations (8 models x 3 technologies x 2 wind speeds x 18 panels). Since this is a gigantic amount of information, only the average values for each case are displayed in this chapter, which reduces the calculations results to 48 – only a single average temperature value for each set of 18 panels. The complete tables with all the singular information are available at the end of this document, in Appendix A. Having said that, table 5.5 shows the values of temperature (in °C) predicted by each model, taking into account each PV technology and the two distinct wind speed values used in CFD simulations, $W_{\text{avg}} = 4.06$ m/s and $W_{\text{max}} = 17.55$ m/s.

Table 5.5: Values of temperature in °C for each set of 18 PV panels.

Technology	**poly-Si**		**CdTe**		**CIGS**	
Wind speed	$W_{\textbf{avg}}$	$W_{\textbf{max}}$	$W_{\textbf{avg}}$	$W_{\textbf{max}}$	$W_{\textbf{avg}}$	$W_{\textbf{max}}$
SA	45		45		47	
Skoplaki 1	36.8078	27.4352	36.5613	27.3261	38.6864	28.2662
Skoplaki 2	37.6965	29.3001	37.4369	29.1637	39.6744	30.3396
Koehl	39.6315	31.0140	44.5293	33.3638	47.3767	35.8964
Mattei 1	39.6433	33.7272	39.2220	33.4452	40.0229	34.0098
Mattei 2	40.6661	33.3382	40.2188	33.0642	41.0599	33.6128
Kurtz	42.3015	35.5083	42.3015	35.5083	42.3015	35.5083
Tamizhmani	42.7761	32.5499	42.7761	32.5499	42.7761	32.5499

By the analysis of the table above, several differences between the temperatures predicted by the panels temperature prediction models for each scenario can be verified. As seen in chapter 3, each model has its characteristic variables, which implies dissimilarity in the final results. Remembering that the Standard Approach is the reference model, which does not account with wind data (it just has an implicit wind velocity of 1 m/s associated), the variation of the temperatures predicted by the models that take wind data into account compared with the standard model is very significant: the maximum absolute variation (worst case) between the results predicted by the complex models is 8.1822 °C, but it is increased to 18.7338 °C when compared with the SA – this type of discrepancy is much more common throughout all the comparisons between the other models with the Standard Approach than with one another.

As it was aforesaid, it is important to mention that models Skoplaki 1, Skoplaki 2, Koehl, Mattei 1 and Mattei 2 take into consideration technology-relative parameters, whereas Kurtz and Tamizhmani do not. This is the reason why the temperatures are the same for the same values of wind speed, disregarding technologies.

By inspection of table 5.5, it is visible that the Skoplaki models predict lower temperatures than the other models for every technology; the Koehl model is the one that exhibits higher variations with the various technologies; the Mattei models present very similar temperatures across all the technologies and the results they generated are identical between both models, never showing a variation of more than 1.037 °C; the Kurtz and Tamizhmani models predicted close temperatures between them for W_{avg}, but differ for higher wind speeds. One interesting case that deviates from all the others is the prediction performed by the Koehl model for the CIGS technology at W_{avg}, which is slightly higher than the value expected by the NOCT formula.

It can be noticed that the predicted temperatures are always lower for W_{max} in contrast to W_{avg}, which clarifies the influence that wind has as a cooling mechanism for solar PV modules. The higher the speed, the lower the temperature predicted according to the module temperature prediction models. These variations in temperature can make all the difference in the output power of the panels, since high temperatures reduce modules efficiency. The variations in output power are shown in the following and last section of this chapter.

5.3 Output Power Variation

As it was discussed before, the efficiency of solar panels decreases with high temperatures. This phenomenon implies lower output powers, which can compromise their operation and their usefulness. In solar plants, where there is a large amount of panels, if this event is multiplied to some extent, the energy production may not match the demand, which is something to be avoided at all costs.

Taking into consideration the temperatures predicted in the previous section, the corresponding output power variations were calculated. Knowing that the SA is the reference model, it can be assumed that its predictions correspond to the temperatures commonly expected and these temperatures correspond to a certain power output variation. Being that all the temperatures predicted by the different models are lower than the ones foreseen by the NOCT formula, except for the case mentioned above, the values displayed in table 5.6 are the difference between the temperatures predicted by the models that take wind data into account and the values anticipated by the Standard Approach multiplied by the temperature coefficient of P_{mpp}. Given that β_{STC} units are %/°C, the results obtained are in percentage. The tables with output power variation for each module can be found in Appendix B.

Table 5.6: Output power variation in percentage (%) for each set of 18 PV panels.

Technology	**poly-Si**		**CdTe**		**CIGS**	
Wind speed	$W_{\mathbf{avg}}$	$W_{\mathbf{max}}$	$W_{\mathbf{avg}}$	$W_{\mathbf{max}}$	$W_{\mathbf{avg}}$	$W_{\mathbf{max}}$
Skoplaki 1	3.19	6.85	2.36	4.95	2.58	5.81
Skoplaki 2	2.85	6.12	2.12	4.43	2.27	5.16
Koehl	2.09	5.45	0.13	3.26	-1.20	3.44
Mattei 1	2.09	4.40	1.62	3.24	2.16	4.03
Mattei 2	1.69	4.55	1.34	3.34	1.84	4.15
Kurtz	1.05	3.70	0.76	2.66	1.46	3.56
Tamizhmani	0.87	4.86	0.62	3.49	1.31	4.48

The interpretation of the table above is that wind speed (W_{avg} or W_{max}) has an influence such that its flow increases/decreases output power in x% when compared with the output power variation normally expected by the SA, in which wind is not taken into consideration.

The analysis of table 5.6 is analogous to the one performed for table 5.5, since one is the consequence of the other. This being said, for the highest variations of temperatures match the highest variations of output power. As it was estimated, the Koehl model predicts an overheating of the panels, decreasing their output power in 1.20% for the CIGS technology when there is a wind speed of 4.06 m/s at the inlet of the wind tunnel. Given that the Skoplaki models showed the biggest decreases of temperatures by wind action, they obviously point to the most beneficial output power variations. Although Kurtz and Tamizhmani models do not take technology-dependent variables, the output power calculations related to them do, which ends the similarities between results for distinct technologies.

In this chapter, the experimental results were showcased. This included the completion of the CFD analysis and the study of data acquired through it. The referred data allowed the verification of the influence of different wind speeds in the temperature of PV panels and how it affects output power, which is a major factor in energy generation of solar plants. To finish, conclusions are drawn in the next and last chapter.

6

Conclusions

Contents

6.1 Conclusions

This dissertation was developed with the main purpose of studying the influence of wind in energy generation of solar plants. To accomplish this task, several parameters were analyzed, which culminated in the decision of giving preference to the investigation of how wind could perform as a natural cooling mechanism for solar photovoltaic modules in solar plants look-alike arrangements of PV arrays. Delving into the several methods one could use to examine the interaction between wind flow and modules temperature, it was decided to follow empirical models that predict panels temperature according to various wind speeds and technology-based parameters (for most of them). Given that technologies present intrinsic properties, the temperatures that would be foreseen would tend to vary from technology to technology. The understanding of this fact led to the choice of three technologies in vogue worldwide (by distinct factors). Due to the fact that it wouldn't be plausible to compare wind flow around geometries of different sizes, it was assumed that all three had exactly the same proportions, but with different parameters that would characterize each of them; since the variables used in the temperature prediction models are technology-related, dimensions could be neglected.

That being said, a Computational Fluid Dynamics analysis of the wind flow around PV geometries was done with the intention of collecting data on wind speeds close to the solar photovoltaic panels. It was observed that for the direction of wind studied, the front rows of photovoltaic arrays always show higher wind velocity magnitudes, which are similar to the ones registered for the tip panels of the rear rows; the occurrence of wind shadowing between rows of panels imply lower wind speeds for most back panels. The referred data were used in the calculations related to the modules temperature predictions that were subsequently crucial to the output power variation results calculated for each scenario. To execute this assignment, it was imperative to use factual wind information that was gathered from reliable sources, thus empowering simulations of concrete circumstances, mimetizing a real-life approach.

The results achieved expose that higher wind speeds are directly related to decreases in modules temperature: for the average wind speeds verified for Lisbon in the year of 2020, variations of output power reached 3.19 percentage points, which expresses a very significant amount of electrical energy production when talking about solar plants. For the highest wind velocities, a maximum variation of 6.85 percentage points in power output was registered. Despite the fact that these last are not the most common values for wind velocities, they are always recorded at some moment, hence their relevance in this research.

One decisive factor that has to be taken into account is that the results attained are highly dependent on the values of wind speeds collected through simulations, on the parameters found in solar panels datasheets and, finally, on the accuracy of the temperature prediction modules employed. To what the wind speeds collected are concerned, the abrupt differences of velocity around the panels influence the calculations made in a critical way. In order to interpret the calculations results displayed in this disserta-

tion correctly, it must be foreknown that the wind speed value collected for each solar photovoltaic panel involve an area right after the surface of the PV panels, where wind speeds have lower magnitudes. This procedure leads to lower temperatures variation and lower output power variations. With this in mind, it can be said that the results here achieved allude to the worst case (although its just-proven benefits), from an electrical engineering perspective.

Taking into consideration the results obtained, it can be said that, in fact, wind works as a natural cooling mechanism for solar panels, thereby improving their productivity, which can lead to significant benefits respecting electrical energy production in solar plants. Nevertheless, several other factors that are correlated with wind loads must be investigated and should not be neglected when thinking about wind influence on solar plants.

To the extent of the reliances explained for the final results herein presented, this thesis cannot be considered a dogma for projects with the same technologies here studied or for every scenario, but it is manifested as a general approach that certainly contributes with a strong insight on how wind influences the electrical energy production in solar plants through its cooling effects.

6.2 Future Work

Throughout the analysis of the experimental results, it was proven that wind can privilege the electrical energy production in solar plants by reducing the temperatures of the photovoltaic modules, thus preventing lower panels efficiencies. Nevertheless, it opens several possible paths for improvements in the future and this is what is discussed in this final section.

The first recommendation has to be the experimental (in-situ) validation of the results calculated by the different module temperature prediction models for the area of Lisbon, concerning irradiances of 800 W/m^2 and ambient temperatures of 20°C to then compare them with the values obtained in this dissertation for the various technologies. Moreover, an investigation that verifies the relationship between wind speeds, pressure influence and dust deposition on solar panels would be of great value, given that these three factors are not independent from each other.

Furthermore, it would be interesting to study how wind affects the output power of circular solar plants (or others designs), whose arrangements of PV arrays are completely distinct from the type of geometries here presented, consequently implying dissimilar wind flows. Also, different wind directions or non-constant irradiances (taking the sun movement into consideration, for example) may contribute to a deeper understanding of the relation between wind and irradiance and its significance when choosing the best site for the construction of a solar plant.

Lastly, an additional research that can be allied to the work developed in this thesis is suggested: an approach on how wind can work as a cooling mechanism on electric cables of solar plants, given that

their overheating reduces the output power, too. This could reinforce the pertinence of using wind as a natural cooling system in solar plants.

All these few ideas may help in the pursue and consolidation of knowledge around the unthinkable number of factors that affect solar plants performance, beyond solar photovoltaic technology-related idiosyncrasies.

Bibliography

[1] E. Comission, "2020 Climate & Energy Package," https://ec.europa.eu/clima/policies/strategies/2020_en, 2020, online; accessed 14 May 2020.

[2] A. P. de Energias Renováveis, "Balanço da produção de eletricidade de portugal continental (abril de 2020)," https://www.apren.pt/pt/energias-renovaveis/producao, 2020, online; accessed 16 May 2020.

[3] IEA (2019), "Renewables 2019," https://www.iea.org/reports/renewables-2019, 2019, online; accessed 14 May 2020.

[4] V. G. Belessiotis and E. Papanicolaou, "History of solar energy," *Comprehensive Renewable Energy*, vol. 3, pp. 85–102, 2012. [Online]. Available: http://dx.doi.org/10.1016/B978-0-08-087872-0.00303-6

[5] U.S. Department of Energy, "The History of Solar," https://www1.eere.energy.gov/solar/pdfs/solar_timeline.pdf, 2019, online; accessed 16 May 2020.

[6] P. Rappaport, "The photovoltaic effect and its utilization," *Solar Energy*, vol. 3, no. 4, p. 8–18, 1959.

[7] J. Simon and J.-J. André, *Molecular Semiconductors: Photoelectrical Properties and Solar Cells*, 1st ed. Springer-Verlag Berlin Heidelberg, 1985.

[8] *Engineering Physics(Be 201)*. McGraw-Hill Education (India) Pvt Limited. [Online]. Available: https://books.google.pt/books?id=u1wql2KActwC

[9] R. D. (auth.), *Introduction to Applied Solid State Physics: Topics in the Applications of Semiconductors, Superconductors, Ferromagnetism, and the Nonlinear Optical Properties of Solids*, 2nd ed. Springer US, 1990. [Online]. Available: http://gen.lib.rus.ec/book/index.php?md5=bbbbd59d22527387fabb8240284fe2fe

[10] T. Soga, *Nanostructured Materials for Solar Energy Conversion*, 1st ed. Elsevier, 2006. [Online]. Available: http://gen.lib.rus.ec/book/index.php?md5=33900c5723410bedd8d5ab86d9da24a6

[11] A. H. M. Smets, K. Jäger, O. Isabella, R. A. van Swaaij, and M. Zeman, *Solar Cell Parameters and Equivalent Circuit*. TU Delft, 2016. [Online]. Available: https://ocw.tudelft.nl/wp-content/uploads/solar_energy_section_9_1_9_3.pdf

[12] J. P. N. Torres, S. K. Nashih, C. A. Fernandes, and J. C. Leite, "The effect of shading on photovoltaic solar panels," *Energy Systems*, vol. 9, no. 1, pp. 195–208, 2018.

[13] S. Nashih, C. Fernandes, J. Torres, J. Gomes, and P. Costa Branco, "Validation of a simulation model for analysis of shading effects on photovoltaic panels," *Journal of Solar Energy Engineering*, vol. 138, no. 4, p. 044503, 2016.

[14] C. F. Fernandes, "Semiconductor junction: a brief review," 2017. [Online]. Available: https://fenix.tecnico.ulisboa.pt/downloadFile/1689468335625622/T5-week3-SEITSF.pdf

[15] J. A. Luceño-Sánchez, A. M. Díez-Pascual, and R. P. Capilla, "Materials for photovoltaics: State of art and recent developments," *International Journal of Molecular Sciences*, vol. 20, no. 4, 2019.

[16] M. Green, Y. Hishikawa, W. Warta, E. Dunlop, D. Levi, J. Hohl-Ebinger, and Ho-Baillie, "A.w.h. solar cell efficiency tables (version 50)," *Prog. Photovolt*, vol. 25, p. 668–676, 2017.

[17] P. Sampaio and M. González, "Photovoltaic solar energy: Conceptual framework," *Renewable and Sustainable Energy Reviews*, vol. 74, p. 590–601, 2017.

[18] U. Gangopadhyay, S. Jana, and S. Das, "State of Art of Solar Photovoltaic Technology," *Conference Papers in Energy*, vol. 2013, pp. 1–9, 2013.

[19] J. Mundo-Hernández, B. De Celis Alonso, J. Hernández-Álvarez, and B. De Celis-Carrillo, "An overview of solar photovoltaic energy in Mexico and Germany," *Renewable and Sustainable Energy Reviews*, vol. 31, pp. 639–649, 2014. [Online]. Available: http://dx.doi.org/10.1016/j.rser.2013.12.029

[20] A. Blakers, N. Zin, K. R. McIntosh, and K. Fong, "High efficiency silicon solar cells," *Energy Procedia*, vol. 33, pp. 1–10, 2013. [Online]. Available: http://dx.doi.org/10.1016/j.egypro.2013.05.033

[21] A. G. Aberle, "Thin-film solar cells," *Thin Solid Films*, vol. 517, no. 17, pp. 4706–4710, 2009.

[22] L. El Chaar, L. A. Lamont, and N. El Zein, "Review of photovoltaic technologies," *Renewable and Sustainable Energy Reviews*, vol. 15, no. 5, pp. 2165–2175, 2011. [Online]. Available: http://dx.doi.org/10.1016/j.rser.2011.01.004

[23] V. Avrutin, N. Izyumskaya, and H. Morko, “Semiconductor solar cells: Recent progress in terrestrial applications,” *Superlattices and Microstructures*, vol. 49, no. 4, pp. 337–364, 2011. [Online]. Available: http://dx.doi.org/10.1016/j.spmi.2010.12.011

[24] G. Conibeer, “Third-generation photovoltaics,” *Mater. Today*, vol. 10, p. 42–50, 2007.

[25] M. Green, “Third generation photovoltaics: Ultra-high conversion efficiency at low cost,” *Progress in Photovoltaics: Research and Applications*, vol. 9, no. 2, p. 123–135, 2001.

[26] A. Martí and A. Luque, “Next generation photovoltaics: High efficiency through full spectrum utilization,” p. 136, 2003.

[27] C. Brabec, “Organic photovoltaics: technology and market,” *Solar Energy Materials and Solar Cells*, vol. 83, no. 2-3, p. 273–292, 2004.

[28] A. Goetzberger, J. Luther, and G. Willeke, “Solar cells: past, present, future,” *Solar Energy Materials and Solar Cells*, vol. 74, no. 1-4, p. 1–11, 2002.

[29] N.-G. Park, “Perovskite solar cells: an emerging photovoltaic technology,” *Materials Today*, vol. 18, no. 2, p. 65–72, 2015.

[30] S. Almosni, A. Delamarre, Z. Jehl, D. Suchet, L. Cojocaru, M. Giteau, and J.-F. Guillemoles, “Material challenges for solar cells in the twenty-first century: directions in emerging technologies,” *Science and Technology of Advanced Materials*, vol. 19, no. 1, p. 336–369, 2018.

[31] A. Luque and A. Martí, “Increasing the efficiency of ideal solar cells by photon induced transitions at intermediate levels,” *Physical Review Letters*, vol. 78, no. 26, p. 5014–5017, 1997.

[32] M. Leite, R. Woo, J. Munday, W. Hong, S. Mesropian, D. Law, and H. Atwater, “Towards an optimized all lattice-matched inalas/ingaasp/ingaas multijunction solar cell with efficiency ¿50%,” *Applied Physics Letters*, vol. 102, no. 3, p. 033901, 2013.

[33] G. Tamizhmani, L. Ji, Y. Tang, L. Petacci, and C. Osterwald, “Photovoltaic module thermal/wind performance : Long-term monitoring and model development for energy rating,” *NCPV and Solar Program Review Meeting*, pp. 936–939, 2003.

[34] H. Ruscheweyh and R. Windhövel, “Wind loads at solar and photovoltaic modules for large plants,” *Proceedings of the 13th International Conference on Wind Engineering*, 2011.

[35] H. Jiang, L. Lu, and K. Sun, “Experimental investigation of the impact of airborne dust deposition on the performance of solar photovoltaic (PV) modules,” *Atmospheric Environment*, vol. 45, no. 25, pp. 4299–4304, 2011. [Online]. Available: http://dx.doi.org/10.1016/j.atmosenv.2011.04.084

[36] A. J. Veldhuis, A. Nobre, T. Reindl, R. Ruther, and A. H. Reinders, “The influence of wind on the temperature of PV modules in tropical environments, evaluated on an hourly basis,” *Conference Record of the IEEE Photovoltaic Specialists Conference*, vol. 31, no. 0, pp. 824–829, 2013.

[37] R. Ross, “Interface design considerations for terrestrial solar cell modules,” in *Proceedings of the 12th IEEE Photovoltaic Specialists Conference*, 1976.

[38] E. Skoplaki, A. Boudouvis, and J. Palyvos, “A simple correlation for the operating temperature of photovoltaic modules of arbitrary mounting,” *Solar Energy Materials and Solar Cells*, vol. 92,1393-1402, 2008.

[39] D. King, W. Boyson, and J. Kratochvill, *Photovoltaic Array Performance Model*. Sandia National Laboratories, 2004.

[40] C. Schwingshackl, M. Petitta, J. E. Wagner, G. Belluardo, D. Moser, M. Castelli, M. Zebisch, and A. Tetzlaff, “Wind effect on PV module temperature: Analysis of different techniques for an accurate estimation,” *Energy Procedia*, vol. 40, pp. 77–86, 2013. [Online]. Available: http://dx.doi.org/10.1016/j.egypro.2013.08.010

[41] L. W. Florschuetz, “Extension of the Hottel-Whillier model to the analysis of combined photovoltaic/thermal flat plate collectors,” *Solar Energy*, vol. 22, no. 4, pp. 361–366, 1979.

[42] T. Markvart, *Solar Electricity*, 2nd ed. Chichester: John Wiley & Sons Ltd., 2000.

[43] E. Skoplaki and J. A. Palyvos, “Operating temperature of photovoltaic modules: A survey of pertinent correlations,” *Renewable Energy*, vol. 34, no. 1, pp. 23–29, 2009.

[44] J. A. Duffie and W. A. Beckman, *Solar Engineering of Thermal Processes*, 4th ed., 2013, vol. 3, no. 3.

[45] S. Armstrong and W. G. Hurley, “A thermal model for photovoltaic panels under varying atmospheric conditions,” *Applied Thermal Engineering*, vol. 30, no. 11-12, pp. 1488–1495, 2010. [Online]. Available: http://dx.doi.org/10.1016/j.applthermaleng.2010.03.012

[46] M. Koehl, M. Heck, S. Wiesmeier, and J. Wirth, “Modeling of the nominal operating cell temperature based on outdoor weathering,” *Solar Energy Materials and Solar Cells*, vol. 95, no. 7, pp. 1638–1646, 2011. [Online]. Available: http://dx.doi.org/10.1016/j.solmat.2011.01.020

[47] D. Faiman, “Assessing the Outdoor Operating Temperature of Photovoltaic Modules,” *Wiley InterScience*, no. 16, pp. 307–315, 2008.

[48] M. Mattei, G. Notton, C. Cristofari, M. Muselli, and P. Poggi, “Calculation of the polycrystalline PV module temperature using a simple method of energy balance,” *Renewable Energy*, vol. 31, no. 4, pp. 553–567, 2006.

[49] S. Kurtz, D. Miller, M. Kempe, N. Bosco, K. Whitefield, M. J. Wohlgemuth, N. Dhere, and T. Zgonena, “Evaluation of High-Temperature Exposure of Photovoltaic Modules: Preprint,” *Nrel*, pp. 2399–2404, 2009. [Online]. Available: http://www.osti.gov/bridge

[50] T. Bhattacharya, A. K. Chakraborty, and K. Pal, “Effects of Ambient Temperature and Wind Speed on Performance of Monocrystalline Solar Photovoltaic Module in Tripura, India,” *Journal of Solar Energy*, vol. 2014, pp. 1–5, 2014.

[51] A. Kilikevičius, A. Čereška, and K. Kilikevičiene, “Analysis of external dynamic loads influence to photovoltaic module structural performance,” *Engineering Failure Analysis*, vol. 66, pp. 445–454, 2016.

[52] K.-A. Weiss, M. Assmus, S. Jack, and M. Koehl, “Measurement and simulation of dynamic mechanical loads on pv-modules,” in *Reliability of Photovoltaic Cells, Modules, Components, and Systems II*, 2009.

[53] J. Amajama, J. C. Ogbulezie, N. A. Akonjom, and Victor C. Onuabuchi, “Impact of wind on the output of photovoltaic panel and solar illuminance/intensity,” *International Journal of Engineering Research and General Science*, vol. 4, no. 5, 2016.

[54] H. H. Hu, “Chapter 10 - Computational Fluid Dynamics,” in *Fluid Mechanics (Fifth Edition)*, 5th ed., P. K. Kundu, I. M. Cohen, and D. R. Dowling, Eds. Boston: Academic Press, 2012, pp. 421–472. [Online]. Available: https://www.sciencedirect.com/science/article/pii/B9780123821003100101

[55] IPMA, “Classificação do vento,” https://www.ipma.pt/pt/educativa/faq/meteorologia/previsao/faqdetail.html?f=/pt/educativa/faq/meteorologia/previsao/faq_0032.html., online; accessed 4 June 2020.

[56] Meteored, “Lisbon weather - historical,” https://www.theweather.com/lisbon.htm?d=historical, online; accessed 30 May 2021.

[57] IPMA, “Publications - monthly climate bulletins,” https://www.ipma.pt/resources.www/docs/im.publicacoes/edicoes.online, online; accessed 30 May 2021.

[58] BYD, “156.57p - series - 4bb,” https://sg.byd.com/wp-content/uploads/2017/10/combine-4-1.pdf, online; accessed 23 April 2021.

[59] F. Solar, “First solar series 4 pv module,” https://www.firstsolar.com/en-Emea/-/media/First-Solar/Technical-Documents/Series-4-Datasheets/Series-4V3-Module-Datasheet.ashx, online; accessed 23 April 2021.

[60] S. Frontier, “Product data sheet sf170-s,” https://www.solar-frontier.com/eng/solutions/products/pdf/datesheat_170.pdf, online; accessed 23 April 2021.

[61] A. T. James Shipman, Jerry D. Wilson, *An Introduction to Physical Science*, 12th ed. Brooks Cole, 2007. [Online]. Available: http://gen.lib.rus.ec/book/index.php?md5=6beb68021c5f43fa797a297f46f83fc6

[62] Latlong, “Lisbon, portugal,” https://www.latlong.net/place/lisbon-portugal-804.html, online; accessed 13 May 2021.

[63] J. Kafka and M. A. Miller, “The dual angle solar harvest (dash) method: An alternative method for organizing large solar panel arrays that optimizes incident solar energy in conjunction with land use,” *Renewable Energy*, vol. 155, pp. 531–546, 2020. [Online]. Available: https://doi.org/10.1016/j.renene.2020.03.025

[64] O. A. de Lisboa, “Solstício de inverno 2020,” https://oal.ul.pt/solsticio-de-inverno-2020/, online; accessed 12 May 2021.

[65] ——, “Crepúsculos, duração do dia, alturas e azimutes do sol (lisboa),” http://oal.ul.pt/documentos/2019/12/creplisboa2020.pdf/, online; accessed 13 May 2021.

[66] NASA, “What are wind tunnels?” https://www.nasa.gov/audience/forstudents/k-4/stories/nasa-knows/what-are-wind-tunnels-k4.html, online; accessed 1 June 2021.

[67] B. Chanetz, “A century of wind tunnels since Eiffel,” *Comptes Rendus - Mecanique*, vol. 345, no. 8, pp. 581–594, 2017. [Online]. Available: http://dx.doi.org/10.1016/j.crme.2017.05.012

[68] Autodesk, “Wind tunnel,” https://knowledge.autodesk.com/search-result/caas/CloudHelp/cloudhelp/ENU/FlowDesign/files/GUID-9B85F4A0-5072-454D-8710-CCFF26507BE9-htm.html, online; accessed 2 June 2021.

[69] S. Group, “Why is meshing important for fluid simulations?” https://simutechgroup.com/why-is-meshing-important-for-fluid-simulations/, online; accessed 3 June 2021.

[70] SimScale, “What are boundary conditions?” https://www.simscale.com/docs/simwiki/numerics-background/what-are-boundary-conditions/, online; accessed 2 June 2021.

[71] Autodesk, "Turbulence," https://knowledge.autodesk.com/support/cfd/learn-explore/caas/CloudHelp/cloudhelp/2019/ENU/SimCFD-UsersGuide/files/GUID-E9E8ACA1-8D49-4A49-8A35-52DB1A2C3E5F-htm.html, online; accessed 5 June 2021.

[72] SimScale, "Turbulence: Which model should i select for my cfd analysis?" https://www.simscale.com/blog/2017/12/turbulence-cfd-analysis/, online; accessed 6 June 2021.

[73] G. Gun Gun Ramdlan, A. I. Siswantara, Budiarso, A. Daryus, and H. Pujowidodo, "Turbulence model and validation of air flow in wind tunnel," *International Journal of Technology*, vol. 7, no. 8, pp. 1362–1371, 2016.

[74] Autodesk, "Two equation turbulence models (tke & ted)," https://knowledge.autodesk.com/support/cfd/learn-explore/caas/CloudHelp/cloudhelp/2021/ENU/SimCFD-Learning/files/Reference-Material/Theoretical-Background/Governing-Equations/Turbulent-Flow/GUID-61C4EB55-362C-48A0-8B22-20F9148D190D-html.html, online; accessed 16 June 2021.

[75] I. Encyclopaedia Britannica, "Eddy," https://www.britannica.com/science/eddy-fluid-mechanics, online; accessed 17 June 2021.

A

Module Temperature Predictions

Across this appendix, there are the tables that supplement the temperatures predicted by the module temperature prediction models, exposed in chapter 5.

Table A.1: Values of temperature (in °C) for the Skoplaki 1 model.

	Skoplaki 1					
Technology	**poly-Si**		**CdTe**		**CIGS**	
Wind Speed	$W_{\mathbf{avg}}$	$W_{\mathbf{max}}$	$W_{\mathbf{avg}}$	$W_{\mathbf{max}}$	$W_{\mathbf{avg}}$	$W_{\mathbf{max}}$
Panel 1	32.6285	24.0299	32.4433	23.9708	34.0400	24.4803
Panel 2	33.3544	24.3895	33.1585	24.3251	34.8470	24.8801
Panel 3	33.5686	24.5166	33.3696	24.4504	35.0852	25.0214
Panel 4	33.7343	24.5719	33.5328	24.5048	35.2693	25.0829
Panel 5	33.7010	24.5737	33.5001	24.5066	35.2324	25.0849
Panel 6	33.6191	24.5572	33.4193	24.4904	35.1413	25.0666
Panel 7	33.4776	24.4842	33.2799	24.4185	34.9840	24.9854
Panel 8	33.4289	24.4085	33.2319	24.3438	34.9298	24.9012
Panel 9	32.8802	24.0611	32.6913	24.0016	34.3198	24.5150
Panel 10	34.8841	24.2667	34.6658	24.2041	36.5477	24.7436
Panel 11	41.2076	31.2820	40.8965	31.1165	43.5779	32.5430
Panel 12	42.0158	33.0261	41.6929	32.8350	44.4765	34.4820
Panel 13	42.1045	32.5025	41.7803	32.3191	44.5751	33.8999
Panel 14	42.3172	32.6149	41.9899	32.4299	44.8116	34.0248
Panel 15	42.0124	32.2172	41.6895	32.0379	44.4727	33.5826
Panel 16	41.7031	32.5018	41.3847	32.3184	44.1288	33.8991
Panel 17	41.2356	31.5222	40.9241	31.3532	43.6090	32.8100
Panel 18	34.6679	24.3068	34.4528	24.2436	36.3073	24.7882
Average	**36.8078**	**27.4352**	**36.5613**	**27.3261**	**38.6864**	**28.2662**

Table A.2: Values of temperature (in °C) for the Skoplaki 2 model.

	Skoplaki 2					
Technology	**poly-Si**		**CdTe**		**CIGS**	
Wind Speed	$W_{\mathbf{avg}}$	$W_{\mathbf{max}}$	$W_{\mathbf{avg}}$	$W_{\mathbf{max}}$	$W_{\mathbf{avg}}$	$W_{\mathbf{max}}$
Panel 1	34.6318	25.6879	34.4172	25.6045	36.2671	26.3237
Panel 2	35.2423	26.1394	35.0188	26.0493	36.9459	26.8256
Panel 3	35.4191	26.2971	35.1929	26.2047	37.1425	27.0009
Panel 4	35.5547	26.3653	35.3265	26.2719	37.2932	27.0768
Panel 5	35.5276	26.3676	35.2998	26.2742	37.2631	27.0793
Panel 6	35.4605	26.3472	35.2337	26.2541	37.1885	27.0567
Panel 7	35.3442	26.2570	35.1191	26.1652	37.0592	26.9564
Panel 8	35.3040	26.1631	35.0795	26.0727	37.0145	26.8519
Panel 9	34.8456	25.7274	34.6278	25.6434	36.5049	26.3676
Panel 10	36.4713	25.9861	36.2297	25.8983	38.3123	26.6552
Panel 11	40.8465	33.4489	40.5407	33.2516	43.1765	34.9521
Panel 12	41.3362	34.9685	41.0233	34.7489	43.7210	36.6415
Panel 13	41.3891	34.5239	41.0754	34.3109	43.7798	36.1472
Panel 14	41.5154	34.6202	41.1998	34.4057	43.9201	36.2542
Panel 15	41.3342	34.2775	41.0213	34.0681	43.7187	35.8733
Panel 16	41.1484	34.5233	40.8382	34.3103	43.5121	36.1466
Panel 17	40.8637	33.6649	40.5577	33.4644	43.1956	35.1921
Panel 18	36.3022	26.0363	36.0631	25.9478	38.1243	26.7110
Average	**37.6965**	**29.3001**	**37.4369**	**29.1637**	**39.6744**	**30.3396**

Table A.3: Values of temperature (in °C) for the Koehl model.

	Koehl					
Technology	**poly-Si**		**CdTe**		**CIGS**	
Wind Speed	$W_{\mathbf{avg}}$	$W_{\mathbf{max}}$	$W_{\mathbf{avg}}$	$W_{\mathbf{max}}$	$W_{\mathbf{avg}}$	$W_{\mathbf{max}}$
Panel 1	36.7375	27.0794	40.6350	28.3985	43.6914	30.4938
Panel 2	37.3402	27.6074	41.4304	29.0437	44.4755	31.2475
Panel 3	37.5134	27.7908	41.6598	29.2684	44.7001	31.5084
Panel 4	37.6459	27.8700	41.8355	29.3654	44.8717	31.6208
Panel 5	37.6194	27.8726	41.8004	29.3687	44.8374	31.6246
Panel 6	37.5539	27.8490	41.7135	29.3397	44.7526	31.5910
Panel 7	37.4401	27.7443	41.5627	29.2113	44.6051	31.4422
Panel 8	37.4006	27.6350	41.5105	29.0774	44.5540	31.2868
Panel 9	36.9493	27.1258	40.9142	28.4551	43.9675	30.5602
Panel 10	38.5334	27.4287	43.0169	28.8250	46.0152	30.9928
Panel 11	42.5772	35.5508	48.5106	39.0801	51.1091	42.1343
Panel 12	43.0111	37.0707	49.1109	41.0743	51.6445	44.1254
Panel 13	43.0577	36.6304	49.1756	40.4940	51.7019	43.5515
Panel 14	43.1689	36.7260	49.3298	40.6198	51.8387	43.6763
Panel 15	43.0093	36.3848	49.1084	40.1713	51.6423	43.2303
Panel 16	42.8451	36.6298	48.8810	40.4932	51.4399	43.5507
Panel 17	42.5925	35.7694	48.5317	39.3653	51.1280	42.4224
Panel 18	38.3707	27.4873	42.7997	28.8967	45.8063	31.0764
Average	**39.6315**	**31.0140**	**44.5293**	**33.3638**	**47.3767**	**35.8964**

Table A.4: Values of temperature (in °C) for the Mattei 1 model.

	Mattei 1					
Technology	**poly-Si**		**CdTe**		**CIGS**	
Wind Speed	$W_{\mathbf{avg}}$	$W_{\mathbf{max}}$	$W_{\mathbf{avg}}$	$W_{\mathbf{max}}$	$W_{\mathbf{avg}}$	$W_{\mathbf{max}}$
Panel 1	38.1697	30.4904	37.7849	30.2823	38.5277	30.7167
Panel 2	38.5150	31.0523	38.1217	30.8320	38.8782	31.2892
Panel 3	38.6121	31.2424	38.2165	31.0179	38.9768	31.4828
Panel 4	38.6858	31.3236	38.2884	31.0973	39.0517	31.5656
Panel 5	38.6712	31.3263	38.2741	31.1000	39.0368	31.5684
Panel 6	38.6347	31.3021	38.2386	31.0763	38.9998	31.5437
Panel 7	38.5711	31.1944	38.1765	30.9709	38.9352	31.4339
Panel 8	38.5490	31.0811	38.1549	30.8601	38.9127	31.3185
Panel 9	38.2924	30.5407	37.9046	30.3315	38.6522	30.7679
Panel 10	39.1662	30.8646	38.7570	30.6484	39.5392	31.0980
Panel 11	41.0978	37.4550	40.6402	37.0875	41.4985	37.8019
Panel 12	41.2832	38.3620	40.8209	37.9725	41.6864	38.7229
Panel 13	41.3029	38.1071	40.8401	37.7238	41.7064	38.4641
Panel 14	41.3496	38.1630	40.8856	37.7783	41.7538	38.5209
Panel 15	41.2824	37.9622	40.8201	37.5824	41.6856	38.3170
Panel 16	41.2127	38.1067	40.7522	37.7235	41.6150	38.4638
Panel 17	41.1044	37.5902	40.6467	37.2195	41.5052	37.9393
Panel 18	39.0799	30.9264	38.6727	30.7088	39.4516	31.1610
Average	**39.6433**	**33.7272**	**39.2220**	**33.4452**	**40.0229**	**34.0098**

Table A.5: Values of temperature (in °C) for the Mattei 2 model.

	Mattei 2					
Technology	**poly-Si**		**CdTe**		**CIGS**	
Wind Speed	$W_{\mathbf{avg}}$	$W_{\mathbf{max}}$	$W_{\mathbf{avg}}$	$W_{\mathbf{max}}$	$W_{\mathbf{avg}}$	$W_{\mathbf{max}}$
Panel 1	38.6274	29.5709	38.2314	29.3826	38.9923	29.7795
Panel 2	39.0875	30.1655	38.6802	29.9644	39.4593	30.3856
Panel 3	39.2179	30.3687	38.8074	30.1633	39.5916	30.5927
Panel 4	39.3171	30.4559	38.9041	30.2486	39.6923	30.6816
Panel 5	39.2973	30.4589	38.8848	30.2515	39.6722	30.6846
Panel 6	39.2483	30.4329	38.8370	30.2260	39.6225	30.6581
Panel 7	39.1628	30.3173	38.7536	30.1129	39.5357	30.5403
Panel 8	39.1331	30.1961	38.7247	29.9944	39.5056	30.4168
Panel 9	38.7902	29.6237	38.3903	29.4343	39.1576	29.8334
Panel 10	39.9695	29.9658	39.5403	29.7690	40.3542	30.1821
Panel 11	42.6997	37.6910	42.2011	37.3178	43.1220	38.0417
Panel 12	42.9711	38.8830	42.4654	38.4807	43.3969	39.2518
Panel 13	43.0001	38.5445	42.4936	38.1505	43.4263	38.9082
Panel 14	43.0689	38.6185	42.5606	38.2227	43.4959	38.9833
Panel 15	42.9700	38.3533	42.4643	37.9640	43.3958	38.7141
Panel 16	42.8678	38.5440	42.3647	38.1501	43.2922	38.9077
Panel 17	42.7094	37.8666	42.2105	37.4891	43.1318	38.2199
Panel 18	39.8514	30.0314	39.4252	29.8332	40.2345	30.2490
Average	**40.6661**	**33.3382**	**40.2188**	**33.0642**	**41.0599**	**33.6128**

Table A.6: Values of temperature (in °C) for the Kurtz model.

	Kurtz					
Technology	**poly-Si**		**CdTe**		**CIGS**	
Wind Speed	$W_{\mathbf{avg}}$	$W_{\mathbf{max}}$	$W_{\mathbf{avg}}$	$W_{\mathbf{max}}$	$W_{\mathbf{avg}}$	$W_{\mathbf{max}}$
Panel 1	40.9779	31.3214	40.9779	31.3214	40.9779	31.3214
Panel 2	41.3101	32.1934	41.3101	32.1934	41.3101	32.1934
Panel 3	41.4023	32.4822	41.4023	32.4822	41.4023	32.4822
Panel 4	41.4718	32.6047	41.4718	32.6047	41.4718	32.6047
Panel 5	41.4580	32.6088	41.4580	32.6088	41.4580	32.6088
Panel 6	41.4236	32.5724	41.4236	32.5724	41.4236	32.5724
Panel 7	41.3634	32.4096	41.3634	32.4096	41.3634	32.4096
Panel 8	41.3424	32.2372	41.3424	32.2372	41.3424	32.2372
Panel 9	41.0967	31.4005	41.0967	31.4005	41.0967	31.4005
Panel 10	41.9173	31.9050	41.9173	31.9050	41.9173	31.9050
Panel 11	43.5801	40.2665	43.5801	40.2665	43.5801	40.2665
Panel 12	43.7296	41.1638	43.7296	41.1638	43.7296	41.1638
Panel 13	43.7454	40.9169	43.7454	40.9169	43.7454	40.9169
Panel 14	43.7828	40.9713	43.7828	40.9713	43.7828	40.9713
Panel 15	43.7290	40.7747	43.7290	40.7747	43.7290	40.7747
Panel 16	43.6730	40.9165	43.6730	40.9165	43.6730	40.9165
Panel 17	43.5855	40.4036	43.5855	40.4036	43.5855	40.4036
Panel 18	41.8382	32.0003	41.8382	32.0003	41.8382	32.0003
Average	**42.3015**	**35.5083**	**42.3015**	**35.5083**	**42.3015**	**35.5083**

Table A.7: Values of temperature (in °C) for the Tamizhmani model.

	Tamizhmani					
Technology	**poly-Si**		**CdTe**		**CIGS**	
Wind Speed	$W_{\mathbf{avg}}$	$W_{\mathbf{max}}$	$W_{\mathbf{avg}}$	$W_{\mathbf{max}}$	$W_{\mathbf{avg}}$	$W_{\mathbf{max}}$
Panel 1	41.2347	25.3689	41.2347	25.3689	41.2347	25.3689
Panel 2	41.6389	27.2775	41.6389	27.2775	41.6389	27.2775
Panel 3	41.7499	27.8798	41.7499	27.8798	41.7499	27.8798
Panel 4	41.8334	28.1310	41.8334	28.1310	41.8334	28.1310
Panel 5	41.8168	28.1394	41.8168	28.1394	41.8168	28.1394
Panel 6	41.7756	28.0650	41.7756	28.0650	41.7756	28.0650
Panel 7	41.7032	27.7296	41.7032	27.7296	41.7032	27.7296
Panel 8	41.6779	27.3699	41.6779	27.3699	41.6779	27.3699
Panel 9	41.3800	25.5479	41.3800	25.5479	41.3800	25.5479
Panel 10	42.3616	26.6618	42.3616	26.6618	42.3616	26.6618
Panel 11	44.2427	40.3472	44.2427	40.3472	44.2427	40.3472
Panel 12	44.4053	41.4617	44.4053	41.4617	44.4053	41.4617
Panel 13	44.4224	41.1598	44.4224	41.1598	44.4224	41.1598
Panel 14	44.4629	41.2267	44.4629	41.2267	44.4629	41.2267
Panel 15	44.4046	40.9843	44.4046	40.9843	44.4046	40.9843
Panel 16	44.3438	41.1593	44.3438	41.1593	44.3438	41.1593
Panel 17	44.2486	40.5207	44.2486	40.5207	44.2486	40.5207
Panel 18	42.2686	26.8669	42.2686	26.8669	42.2686	26.8669
Average	**42.7761**	**32.5499**	**42.7761**	**32.5499**	**42.7761**	**32.5499**

B

Output Power Variations

Across this appendix, there are the tables that supplement the output power variations calculated according to the temperatures predicted, as exposed in chapter 5. These results are not in percentage.

Table B.1: Output power variation for the Skoplaki 1 model.

	Skoplaki 1					
Technology	**poly-Si**		**CdTe**		**CIGS**	
Wind Speed	$W_{\mathbf{avg}}$	$W_{\mathbf{max}}$	$W_{\mathbf{avg}}$	$W_{\mathbf{max}}$	$W_{\mathbf{avg}}$	$W_{\mathbf{max}}$
Panel 1	0.0482	0.0818	0.0352	0.0589	0.0402	0.0698
Panel 2	0.0454	0.0804	0.0332	0.0579	0.0377	0.0686
Panel 3	0.0446	0.0799	0.0326	0.0575	0.0369	0.0681
Panel 4	0.0439	0.0797	0.0321	0.0574	0.0364	0.0679
Panel 5	0.0441	0.0797	0.0322	0.0574	0.0365	0.0679
Panel 6	0.0444	0.0797	0.0324	0.0574	0.0368	0.0680
Panel 7	0.0449	0.0800	0.0328	0.0576	0.0372	0.0682
Panel 8	0.0451	0.0803	0.0330	0.0578	0.0374	0.0685
Panel 9	0.0473	0.0817	0.0345	0.0588	0.0393	0.0697
Panel 10	0.0395	0.0809	0.0289	0.0582	0.0324	0.0690
Panel 11	0.0148	0.0535	0.0115	0.0389	0.0106	0.0448
Panel 12	0.0116	0.0467	0.0093	0.0341	0.0078	0.0388
Panel 13	0.0113	0.0487	0.0090	0.0355	0.0075	0.0406
Panel 14	0.0105	0.0483	0.0084	0.0352	0.0068	0.0402
Panel 15	0.0117	0.0499	0.0093	0.0363	0.0078	0.0416
Panel 16	0.0129	0.0487	0.0101	0.0355	0.0089	0.0406
Panel 17	0.0147	0.0526	0.0114	0.0382	0.0105	0.0440
Panel 18	0.0403	0.0807	0.0295	0.0581	0.0331	0.0689
Average	**0.0319**	**0.0685**	**0.0236**	**0.0495**	**0.0258**	**0.0581**

Table B.2: Output power variation for the Skoplaki 2 model.

	Skoplaki 2					
Technology	**poly-Si**		**CdTe**		**CIGS**	
Wind Speed	$W_{\mathbf{avg}}$	$W_{\mathbf{max}}$	$W_{\mathbf{avg}}$	$W_{\mathbf{max}}$	$W_{\mathbf{avg}}$	$W_{\mathbf{max}}$
Panel 1	0.0404	0.0753	0.0296	0.0543	0.0333	0.0641
Panel 2	0.0381	0.0736	0.0279	0.0531	0.0312	0.0625
Panel 3	0.0374	0.0729	0.0275	0.0526	0.0306	0.0620
Panel 4	0.0368	0.0727	0.0271	0.0524	0.0301	0.0618
Panel 5	0.0369	0.0727	0.0272	0.0524	0.0302	0.0618
Panel 6	0.0372	0.0727	0.0273	0.0525	0.0304	0.0618
Panel 7	0.0377	0.0731	0.0277	0.0527	0.0308	0.0621
Panel 8	0.0378	0.0735	0.0278	0.0530	0.0310	0.0625
Panel 9	0.0396	0.0752	0.0290	0.0542	0.0325	0.0640
Panel 10	0.0333	0.0742	0.0246	0.0535	0.0269	0.0631
Panel 11	0.0162	0.0450	0.0125	0.0329	0.0119	0.0373
Panel 12	0.0143	0.0391	0.0111	0.0287	0.0102	0.0321
Panel 13	0.0141	0.0409	0.0110	0.0299	0.0100	0.0336
Panel 14	0.0136	0.0405	0.0106	0.0297	0.0095	0.0333
Panel 15	0.0143	0.0418	0.0111	0.0306	0.0102	0.0345
Panel 16	0.0150	0.0409	0.0117	0.0299	0.0108	0.0336
Panel 17	0.0161	0.0442	0.0124	0.0323	0.0118	0.0366
Panel 18	0.0339	0.0740	0.0250	0.0533	0.0275	0.0629
Average	**0.0285**	**0.0612**	**0.0212**	**0.0443**	**0.0227**	**0.0516**

Table B.3: Output power variation for the Koehl model.

	Koehl					
Technology	**poly-Si**		**CdTe**		**CIGS**	
Wind Speed	$W_{\mathbf{avg}}$	$W_{\mathbf{max}}$	$W_{\mathbf{avg}}$	$W_{\mathbf{max}}$	$W_{\mathbf{avg}}$	$W_{\mathbf{max}}$
Panel 1	0.0322	0.0699	0.0122	0.0465	0.0103	0.0512
Panel 2	0.0299	0.0678	0.0100	0.0447	0.0078	0.0488
Panel 3	0.0292	0.0671	0.0094	0.0440	0.0071	0.0480
Panel 4	0.0287	0.0668	0.0089	0.0438	0.0066	0.0477
Panel 5	0.0288	0.0668	0.0090	0.0438	0.0067	0.0477
Panel 6	0.0290	0.0669	0.0092	0.0438	0.0070	0.0478
Panel 7	0.0295	0.0673	0.0096	0.0442	0.0074	0.0482
Panel 8	0.0296	0.0677	0.0098	0.0446	0.0076	0.0487
Panel 9	0.0314	0.0697	0.0114	0.0463	0.0094	0.0510
Panel 10	0.0252	0.0685	0.0056	0.0453	0.0031	0.0496
Panel 11	0.0094	0.0369	-0.0098	0.0166	-0.0127	0.0151
Panel 12	0.0078	0.0309	-0.0115	0.0110	-0.0144	0.0089
Panel 13	0.0076	0.0326	-0.0117	0.0126	-0.0146	0.0107
Panel 14	0.0071	0.0323	-0.0121	0.0123	-0.0150	0.0103
Panel 15	0.0078	0.0336	-0.0115	0.0135	-0.0144	0.0117
Panel 16	0.0084	0.0326	-0.0109	0.0126	-0.0138	0.0107
Panel 17	0.0094	0.0360	-0.0099	0.0158	-0.0128	0.0142
Panel 18	0.0259	0.0683	0.0062	0.0451	0.0037	0.0494
Average	**0.0209**	**0.0545**	**0.0013**	**0.0326**	**-0.0012**	**0.0344**

Table B.4: Output power variation for the Mattei 1 model.

	Mattei 1					
Technology	**poly-Si**		**CdTe**		**CIGS**	
Wind Speed	$W_{\mathbf{avg}}$	$W_{\mathbf{max}}$	$W_{\mathbf{avg}}$	$W_{\mathbf{max}}$	$W_{\mathbf{avg}}$	$W_{\mathbf{max}}$
Panel 1	0.0266	0.0566	0.0202	0.0412	0.0263	0.0505
Panel 2	0.0253	0.0544	0.0193	0.0397	0.0252	0.0487
Panel 3	0.0249	0.0537	0.0190	0.0391	0.0249	0.0481
Panel 4	0.0246	0.0533	0.0188	0.0389	0.0246	0.0478
Panel 5	0.0247	0.0533	0.0188	0.0389	0.0247	0.0478
Panel 6	0.0248	0.0534	0.0189	0.0390	0.0248	0.0479
Panel 7	0.0251	0.0538	0.0191	0.0393	0.0250	0.0483
Panel 8	0.0252	0.0543	0.0192	0.0396	0.0251	0.0486
Panel 9	0.0262	0.0564	0.0199	0.0411	0.0259	0.0503
Panel 10	0.0228	0.0551	0.0175	0.0402	0.0231	0.0493
Panel 11	0.0152	0.0294	0.0122	0.0222	0.0171	0.0285
Panel 12	0.0145	0.0259	0.0117	0.0197	0.0165	0.0257
Panel 13	0.0144	0.0269	0.0116	0.0204	0.0164	0.0265
Panel 14	0.0142	0.0267	0.0115	0.0202	0.0163	0.0263
Panel 15	0.0145	0.0274	0.0117	0.0208	0.0165	0.0269
Panel 16	0.0148	0.0269	0.0119	0.0204	0.0167	0.0265
Panel 17	0.0152	0.0289	0.0122	0.0218	0.0170	0.0281
Panel 18	0.0231	0.0549	0.0177	0.0400	0.0234	0.0491
Average	**0.0209**	**0.0440**	**0.0162**	**0.0324**	**0.0216**	**0.0403**

Table B.5: Output power variation for the Mattei 2 model.

	Mattei 2					
Technology	**poly-Si**		**CdTe**		**CIGS**	
Wind Speed	$W_{\mathbf{avg}}$	$W_{\mathbf{max}}$	$W_{\mathbf{avg}}$	$W_{\mathbf{max}}$	$W_{\mathbf{avg}}$	$W_{\mathbf{max}}$
Panel 1	0.0249	0.0602	0.0190	0.0437	0.0248	0.0534
Panel 2	0.0231	0.0579	0.0177	0.0421	0.0234	0.0515
Panel 3	0.0226	0.0571	0.0173	0.0415	0.0230	0.0509
Panel 4	0.0222	0.0567	0.0171	0.0413	0.0227	0.0506
Panel 5	0.0222	0.0567	0.0171	0.0413	0.0227	0.0506
Panel 6	0.0224	0.0568	0.0173	0.0414	0.0229	0.0507
Panel 7	0.0228	0.0573	0.0175	0.0417	0.0231	0.0510
Panel 8	0.0229	0.0577	0.0176	0.0420	0.0232	0.0514
Panel 9	0.0242	0.0600	0.0185	0.0436	0.0243	0.0532
Panel 10	0.0196	0.0586	0.0153	0.0426	0.0206	0.0521
Panel 11	0.0090	0.0285	0.0078	0.0215	0.0120	0.0278
Panel 12	0.0079	0.0239	0.0071	0.0183	0.0112	0.0240
Panel 13	0.0078	0.0252	0.0070	0.0192	0.0111	0.0251
Panel 14	0.0075	0.0249	0.0068	0.0190	0.0109	0.0249
Panel 15	0.0079	0.0259	0.0071	0.0197	0.0112	0.0257
Panel 16	0.0083	0.0252	0.0074	0.0192	0.0115	0.0251
Panel 17	0.0089	0.0278	0.0078	0.0210	0.0120	0.0272
Panel 18	0.0201	0.0584	0.0156	0.0425	0.0210	0.0519
Average	**0.0169**	**0.0455**	**0.0134**	**0.0334**	**0.0184**	**0.0415**

Table B.6: Output power variation for the Kurtz model.

	Kurtz					
Technology	**poly-Si**		**CdTe**		**CIGS**	
Wind Speed	$W_{\mathbf{avg}}$	$W_{\mathbf{max}}$	$W_{\mathbf{avg}}$	$W_{\mathbf{max}}$	$W_{\mathbf{avg}}$	$W_{\mathbf{max}}$
Panel 1	0.0157	0.0533	0.0113	0.0383	0.0187	0.0486
Panel 2	0.0144	0.0499	0.0103	0.0359	0.0176	0.0459
Panel 3	0.0140	0.0488	0.0101	0.0350	0.0174	0.0450
Panel 4	0.0138	0.0483	0.0099	0.0347	0.0171	0.0446
Panel 5	0.0138	0.0483	0.0099	0.0347	0.0172	0.0446
Panel 6	0.0139	0.0485	0.0100	0.0348	0.0173	0.0447
Panel 7	0.0142	0.0491	0.0102	0.0353	0.0175	0.0452
Panel 8	0.0143	0.0498	0.0102	0.0357	0.0175	0.0458
Panel 9	0.0152	0.0530	0.0109	0.0381	0.0183	0.0484
Panel 10	0.0120	0.0511	0.0086	0.0367	0.0158	0.0468
Panel 11	0.0055	0.0185	0.0040	0.0133	0.0106	0.0209
Panel 12	0.0050	0.0150	0.0036	0.0107	0.0101	0.0181
Panel 13	0.0049	0.0159	0.0035	0.0114	0.0101	0.0189
Panel 14	0.0047	0.0157	0.0034	0.0113	0.0100	0.0187
Panel 15	0.0050	0.0165	0.0036	0.0118	0.0101	0.0193
Panel 16	0.0052	0.0159	0.0037	0.0114	0.0103	0.0189
Panel 17	0.0055	0.0179	0.0040	0.0129	0.0106	0.0204
Panel 18	0.0123	0.0507	0.0089	0.0364	0.0160	0.0465
Average	**0.0105**	**0.0370**	**0.0076**	**0.0266**	**0.0146**	**0.0356**

Table B.7: Output power variation for the Tamizhmani model.

	Tamizhmani					
Technology	**poly-Si**		**CdTe**		**CIGS**	
Wind Speed	$W_{\mathbf{avg}}$	$W_{\mathbf{max}}$	$W_{\mathbf{avg}}$	$W_{\mathbf{max}}$	$W_{\mathbf{avg}}$	$W_{\mathbf{max}}$
Panel 1	0.0147	0.0766	0.0105	0.0550	0.0179	0.0671
Panel 2	0.0131	0.0691	0.0094	0.0496	0.0166	0.0611
Panel 3	0.0127	0.0668	0.0091	0.0479	0.0163	0.0593
Panel 4	0.0123	0.0658	0.0089	0.0472	0.0160	0.0585
Panel 5	0.0124	0.0658	0.0089	0.0472	0.0161	0.0585
Panel 6	0.0126	0.0660	0.0090	0.0474	0.0162	0.0587
Panel 7	0.0129	0.0674	0.0092	0.0484	0.0164	0.0597
Panel 8	0.0130	0.0688	0.0093	0.0494	0.0165	0.0609
Panel 9	0.0141	0.0759	0.0101	0.0545	0.0174	0.0665
Panel 10	0.0103	0.0715	0.0074	0.0513	0.0144	0.0630
Panel 11	0.0030	0.0181	0.0021	0.0130	0.0085	0.0206
Panel 12	0.0023	0.0138	0.0017	0.0099	0.0080	0.0172
Panel 13	0.0023	0.0150	0.0016	0.0108	0.0080	0.0181
Panel 14	0.0021	0.0147	0.0015	0.0106	0.0079	0.0179
Panel 15	0.0023	0.0157	0.0017	0.0112	0.0080	0.0186
Panel 16	0.0026	0.0150	0.0018	0.0108	0.0082	0.0181
Panel 17	0.0029	0.0175	0.0021	0.0125	0.0085	0.0201
Panel 18	0.0107	0.0707	0.0076	0.0508	0.0147	0.0624
Average	**0.0087**	**0.0486**	**0.0062**	**0.0349**	**0.0131**	**0.0448**